AN ABSTRACT OF THE THESIS OF

Samantha K. Cargill for the degree of Master of Science in Water Resources Science presented on November 25, 2019.

Title: The Influence of Lithology on Stream Metabolism in Mountain Systems

Abstract approved:

_____

Catalina Segura

Physical disturbance in streams has important effects on the metabolic rates of gross primary production (GPP) and ecosystem respiration (ER). Underlying lithology can control sediment size, amount, and evolution in the stream, influencing substrate stability and its effect on benthic organisms. We assessed the patterns of disturbance and recovery of metabolic rates after periods of increased flow and suspended sediment flux in different lithologies. We modeled whole-stream metabolism during the winter-spring period between December and April in two streams in the Oregon Coast Range: one with basalt lithology, and one with sandstone lithology. Our results indicated that the two streams varied in their patterns of response and recovery to storms. Both streams were heterotrophic during the entirety of the study period, but changes in heterotrophy were driven by changes in ER. Post-storm GPP decreased in both streams, but the basalt basin had greater proportional decreases. Decreases were also greater later in the study period, when pre-storm rates of GPP were higher. Rates of ER increased in the basalt basin post-storm and did not change from pre- to post-storm in the sandstone basin. Recovery of GPP was more rapid in the sandstone basin than the basalt basin. The P/R ratio recovery period was similar in both streams, but recovery was faster in the sandstone basin. Overall, our results indicated that the underlying lithology of small mountain streams drives variability in heterotrophy through differing effects on ER.

The Influence of Lithology on Stream Metabolism in Mountain Systems

by
Samantha K. Cargill

A THESIS

submitted to

Oregon State University

in partial fulfillment of
the requirements for the
degree of

Master of Science

Presented November 25, 2019
Commencement June 2020

Master of Science thesis of Samantha K. Cargill presented on November 25, 2019

APPROVED:

Major Professor, representing Water Resources Science

Director of the Water Resources Graduate Program

Dean of the Graduate School

I understand that my thesis will become part of the permanent collection of Oregon State University libraries. My signature below authorizes release of my thesis to any reader upon request.

Samantha K. Cargill, Author

ACKNOWLEDGEMENTS

I would first like to express my gratitude to my advisors, Catalina Segura and Dana Warren, for their support and guidance over the course of this project. Their enthusiasm, patience, and understanding have helped me improve as a scientist and researcher. The time and care they put into not only my research but also my development as a person has been greatly appreciated.

Thank you to Cait Harriett, Allie Johnson, Emily Crampe, and Nora Boylan, without whom I would never have been able to finish. Your friendship and encouragement have helped me through the challenges of graduate school, and your reminders to have fun have kept me sane. To my housemates Kate Kouba and Lety Cavazos Sanchez, thank you for your perspective and for listening to me sort out my thoughts over tacos. To my officemates Arianna Goodman, Karla Jarecke, Ryan Cole, and Adam Pate, thank you for the many conversations and late nights in Snell. To my labmate Allie Swartz, thank you for your help with fieldwork and your advice.

I appreciated field and lab assistance from Joey Tinker, Katie Scherr, Cory Mack, Rosemary Pazdral, Kylie Brooks, Emily Heaston, and Jon Sanfilippo; I am grateful for all the times you spent outside in the rain, wading in the stream and fighting stinging nettle with me. Without your help, we would not have been able to collect all the data we did. Thank you to my committee member Dr. Gordon Grant for his feedback, and to Dr. Lily Ranjbar for being my graduate council representative. Thank you also to Dr. Mary Santelmann and Dr. Carlos Gonzalez, who shared data to fill gaps in our records. Thank you in particular to Mary, for your efforts to make sure every water resources student is supported and successful. I thank the administrative staff of FERM – Madison Dudley and Chelsey Durling – and the WRGP – Annie Ingersoll and Catherine Mullins – for always taking the time to answer my questions and help keep me on the right track. Thank you to the National Science Foundation, who funded this project, and to the OSU Graduate School and the College of Forestry for additional support.

Lastly, I would like to thank my family for their love and support over the past several years. Though they live on the opposite coast, they were always available to talk, even when the time difference meant it was the next day for them. To my parents: thank you for instilling in me a love of science and the outdoors. Without your example of hard work and your encouragement to be my best, I wouldn't be where I am today.

TABLE OF CONTENTS

LIST OF FIGURES

LIST OF FIGURES (Continued)

LIST OF TABLES

LIST OF APPENDICES

LIST OF APPENDIX FIGURES

LIST OF APPENDIX FIGURES (Continued)

Figure Page

LIST OF APPENDIX TABLES

1 Introduction

Key stream ecosystem functions, such as the cycling of carbon and nutrients and food web dynamics, are influenced by the metabolic processes of primary production and respiration (Bernhardt et al., 2018). Gross primary production (GPP) is the total fixation of inorganic carbon to organic carbon by photoautotrophs in the stream, converting solar energy to carbohydrates. Ecosystem respiration (ER) is the production of energy by stream organisms, both autotrophs and heterotrophs from the oxidation of organic carbon. The rates of primary production and respiration are rarely in balance; in net autotrophic streams, there is more primary production than ecosystem respiration, while in net heterotrophic streams, ecosystem respiration is greater than in-stream production. The metabolic status of a stream provides information about system resources and energy cycles. In headwater streams, benthic algae are the main primary producers (Power & Dietrich, 2002), and a great deal of research has been conducted to explore factors that limit or control the rates of autotrophy by benthic algae. Temperature, nutrient status and light availability are recognized as the dominant abiotic factors affecting stream metabolism (Larned, 2010), but the frequency and size of high flow events that influence substrate stability in streams and rivers can also affect metabolic rates and community composition of benthic algal communities.

Three main processes physically disturb the benthic biofilms in streams during high flow events: removal of material by the flow of water (Biggs & Thomsen, 1995), abrasion of material by small particles (sand) (Luce et al., 2013), and overturning of the substrate itself, which can both abrade material and shade any remaining material, thereby impacting the capacity for primary production even if the biofilms remain on a given rock (Biggs & Close, 1989; Biggs et al., 1999). Lithology controls sediment size, amount, and evolution in the channel (Mueller et al., 2016; O'Connor et al., 2014). Motion of sediment in streams is spatially variable (Lisle et al., 2000; Segura & Pitlick, 2015), which leads to variable responses of benthic periphyton (Katz et al., 2018; Segura et al., 2011; Uehlinger et al., 2003). Abrasion due to mobilization of smaller particles is possible at moderate flows, without movement of larger grains (Luce et al., 2010). Abundance of small particles enhances the movement of all size fractions (Curran & Wilcock, 2005; Wilcock et al., 2001). Therefore, in systems with more fine highly mobile sediment, stream metabolism –

particularly the GPP component of metabolism – may be more susceptible to ecosystem level impacts from moderate and higher flow events. This expectation has been borne out in urbanized systems where a combination of higher flows and smaller sediment create susceptible systems (Blaszczak et al., 2019; Qasem et al., 2019). But this has not been explored in forested systems where the effects of urbanization on substrate size distributions are absent. Across a range of natural landscapes, Mueller and Pitlick (2013) found that relative sediment supply was dominated by the lithology of the basin, and that sediment concentrations increase as lithology becomes softer. As a result, underlying lithology of forested streams systems may be an important factor controlling stream metabolism, with softer lithologies that generate more sediment expected to have more mobility events and therefore experience larger and more frequent impacts to metabolism.

Earlier studies explored the effects of physical disturbance on algal communities and standing stocks. O'Connor et al. (2012) found that while larger flood pulses destroyed bed habitat and resulted in increased recovery times of benthic organisms, small pulses that did not disturb the bed but increased turbidity resulted in faster recovery times after flood events. Biggs and Thomsen (1995) found that spates without bedload movement could have varying magnitudes of disturbance to the benthic biofilms due to different resistances of periphyton communities. Several studies identify losses in biomass due to increased flow (Biggs, 1995; Biggs & Close, 1989; Clausen & Biggs, 1997; Tett et al., 1978); others concluded that adding sediment to high flows in experiments further disturbed benthic organisms (Francoeur & Biggs, 2006). Several studies found that periphyton taxonomic makeup can also play a role in the resilience and resistance of the communities due to disturbance (Biggs & Thomsen, 1995; Francoeur & Biggs, 2006; Grimm & Fisher, 1989; Peterson & Stevenson, 1992). However, metabolic rates are not always well-predicted by biomass of benthic periphyton (Izagirre et al., 2008; Uehlinger & Naegeli, 1998).

Recent advances in measuring and modeling stream GPP and ER over long time periods have allowed researchers to study the bioenergetics of the whole system, not just algal communities. Metabolic rates can be modeled based on measurements of daily changes in dissolved oxygen concentrations (Appling et al., 2018; Holtgrieve et al., 2010; Odum, 1956). Several studies found that floods decreased rates of GPP more than rates of

ER (Qasem et al., 2019; Uehlinger, 2006). The time of year also affects patterns in metabolism (Roberts et al., 2007; Uehlinger, 2000, 2006; Uehlinger et al., 2003).

Controls on metabolic rates other than substrate stability are light (Acuña et al., 2004; Roberts et al., 2007), nutrient concentrations, and temperature (Hill et al., 2000; Larned, 2010). However, our current understanding of the interactions between controls of metabolic rates is limited (Bernhardt et al., 2018; Bernot et al., 2010; McDowell, 2015). In forested headwater streams, shading is a particularly important factor controlling primary production and therefore overall stream metabolic rates. With this high shading and with an input of external fixed carbon from adjacent terrestrial systems, headwaters are expected to be net heterotrophic (Vannote et al., 1980). However, even in systems where light is high and nutrient resources are not limiting, bed instability can result in low rates of GPP (Atkinson et al., 2008; Uehlinger et al., 2002). Recent studies in urban systems have found that as stream flashiness increased, light was less explanatory as a variable controlling metabolic rates (Blaszczak et al., 2019). The history of disturbance in the stream also affects stream resilience and recovery, where responses vary based on the development state of the community and the stresses under which the community grows (Katz et al., 2018; Peterson & Stevenson, 1992).

The goals of this study were to explore the limiting effects of suspended sediment and increased flow on metabolic rates in two basins with contrasting lithologies (sandstone- and basalt-dominated), compare metabolic rates before and after storms, and compare patterns of metabolism between the two streams. Our expectations were that in the more friable sandstone basin, the GPP and ER in the system would be disturbed and reset more often than the GPP and ER in the stream in the basalt basin given the more frequent movement of small sand particles in the sandstone basin that can cause abrasion to biofilm mats, even at moderate flows.

2 Study Sites

This study was conducted in two streams with contrasting lithology in the Oregon Coast Range (Figure 2.1). In an effort to isolate the effects of lithology on primary production, the stream reaches chosen for the study were similar in size, land cover, slope, channel form (pool-riffle morphology), and climate. The Oregon Coast Range has a Mediterranean climate, with wet winters and mild summers. While the overall climate regime is the same, annual precipitation is slightly higher in the stream reach closer to the coast (PRISM Climate Group, Oregon State University, http://prism.oregonstate.edu/, created 12 October 2019) (Table 2.1). Both watersheds are forested, with upland forests dominated by stands of mid-succession Douglas fir (*Pseudotsuga menziesii*).

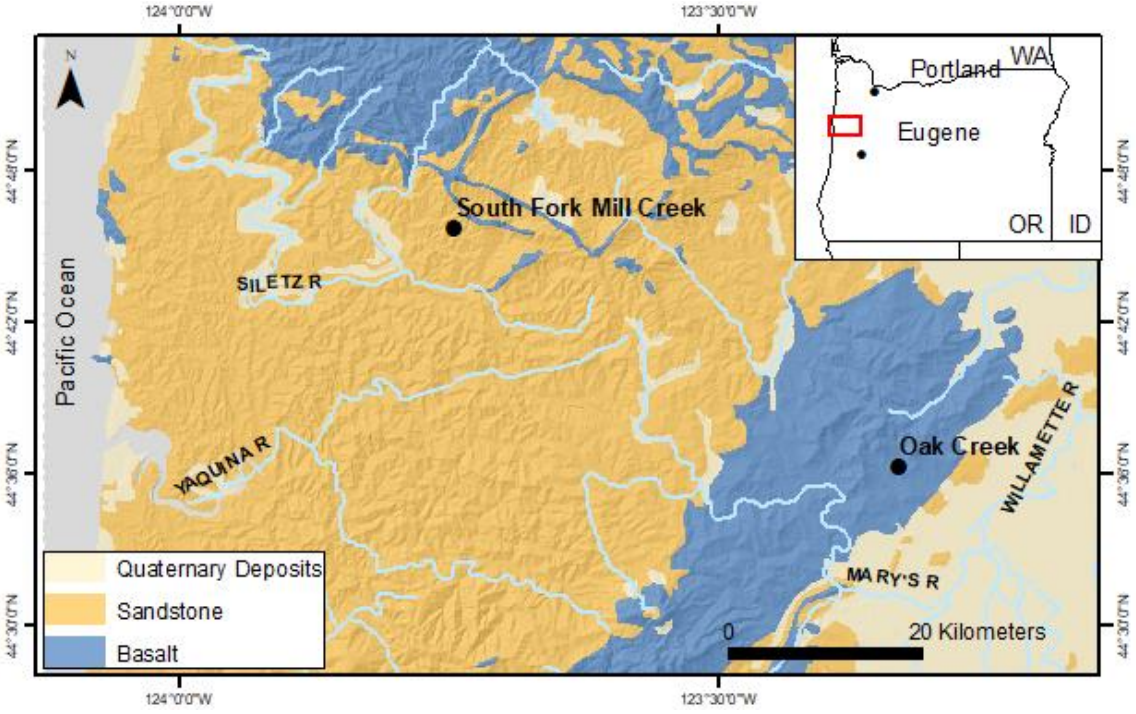

Figure 2.1 Location map of the two study streams. Both streams are in the Oregon Coast Range. Oak Creek is underlain by basalt, while South Fork Mill Creek is underlain by sandstone (Walker & MacLeod, 1991).

The first study site is a 160-meter reach in Oak Creek, a stream underlain by basaltic lithology (Milhous, 1973; O'Connor et al., 2014). Oak Creek is located in the McDonald-Dunn forest in the eastern foothills of the Oregon Coast Range in Corvallis, OR. Upper canopy riparian vegetation includes big leaf maple (*Acer macrophyllus*), alder (*Alnus sp*),

and black cottonwood (*Papulus trichocarpa*), while the understory riparian vegetation includes willow (*Salix sp*), blackberry (*Rubus armeniacus*), and salmonberry (*Rubus spectabilis*). The study reach has a bankfull discharge of 3.41 m^3/s, a bankfull width of 6 m, and a slope of 0.014 m/m, with a contributing drainage area of about 6.7 km^2 (Katz et al., 2018). The median grain size (D_{50}) of the channel bed surface is 47.6 mm, the D_{16} is 21.2 mm, and the D_{84} is 84.6 mm (Katz et al., 2018) (Figure 2.2). The mean stream winter nitrate nitrogen concentration in 2019 was 176.7 $\mu g\ L^{-1}$ (N = 5), while the mean stream winter phosphate phosphorus concentration was 18.46 $\mu g\ L^{-1}$ (Table 2.1).

The second study site is a 160-meter reach in the South Fork Mill Creek, a tributary of the Siletz River located 37 km west of Oak Creek in the central Coast Range of Oregon. This stream is underlain by the Tyee formation, a sequence of sandstone and siltstone lithologies (Snavely et al., 1964). The riparian vegetation is primary deciduous, including vine maple (*Acer circinatum*), red alder (*Alnus rubra*), and black cottonwood (*Populus trichocarpa*). The understory includes a thick layer of ferns, grasses, stinging nettle (*Urtica dioica*), and salmonberry (*Rubus spectabilis*). The study reach has a bankfull discharge of 2.5 m^3/s, a bankfull width of 7 m, and a slope of 0.009 m/m, with a contributing drainage area of about 4.3 km^2 (Bair et al., 2019). The D_{50} of the surface is 28.6 mm, the D_{16} is 12.4 mm, and the D_{84} is 56.9 mm (Figure 2.2). The mean winter nitrate nitrogen concentration (N = 4) in the 2019 water year was 938.9 $\mu g\ L^{-1}$, while the mean winter phosphate phosphorus concentration was 6.8 $\mu g\ L^{-1}$ (Table 2.1).

Table 2.1 Reach characteristics of study sites in the two focal streams in western Oregon, Oak Creek and South Fork Mill Creek. Values in parentheses are standard deviations.

Characteristic	Oak Creek	South Fork Mill Creek
Bankfull Discharge ($m^3\ s^{-1}$)	3.41	2.5
Bankfull Width (m)	5.6 ± 0.2	7.4 ± 1.6
D_{50} (mm)	47.6 ± 1.8	28.6 ± 1.5
Slope (m/m)	0.014	0.009
[NO_3^- – N] ($\mu g\ L^{-1}$)	176.7 (61.2)	938.9 (106.9)
[PO_4^{-3} – P] ($\mu g\ L^{-1}$)	18.46 (4.4)	6.8 (0.7)
Mean Annual Precipitation, 1997-2018 (mm)	1,623.83	1,978.98
Drainage Area (km^2)*	6.7	4.3
Coordinates (latitude, longitude)	44° 36’ 17.9532”, -123° 19’ 59.5632”	44° 45’ 43.0302”, -123° 44’ 44.7678”

* Derived from Oregon Spatial Data Library, https://gis.dogami.oregon.gov/arcgis/rest/services/Public/BareEarth/ImageServer, accessed September 8, 2018.

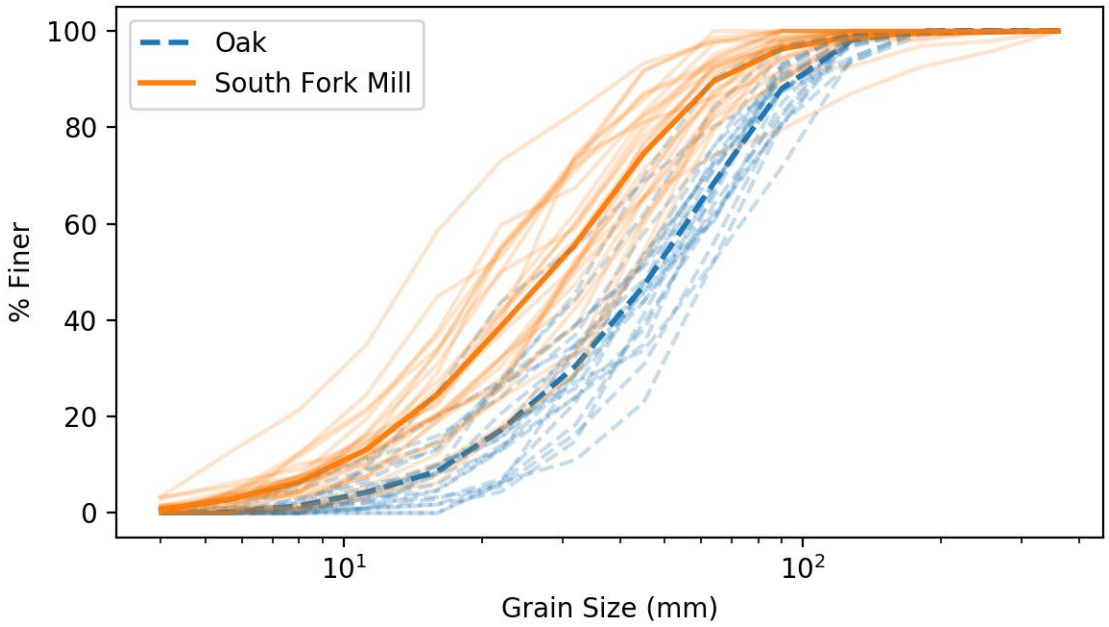

Figure 2.2 Surface grain size distributions (with mean distributions shown as bolded lines) of South Fork Mill Creek (sandstone, orange) and Oak Creek (basalt, blue). South Fork Mill Creek has a finer grain size distribution than Oak Creek. The D_{50} of South Fork Mill Creek is 28.6 mm, while the D_{50} of Oak Creek is 47.6 mm.

3 Methods

3.1 Data Collection

3.1.1 Metabolism Data

Stream metabolism encompasses gross primary production and ecosystem respiration within a given stream. Metabolism is calculated from the diurnal shifts in dissolved oxygen in a stream that represent production and consumption of oxygen by stream autotrophs and stream heterotrophs. Along with dissolved oxygen concentrations, stream metabolism estimates also require data on (1) stream light, (2) water temperature, (3) air pressure, and (4) oxygen exchange rates with the atmosphere. In Oak Creek, data loggers were deployed to quantify and record light, temperature, and dissolved oxygen from December 2017 to April 2018 and from December 2018 to April 2019. In South Fork Mill Creek loggers were deployed from December 2018 to April 2019 (Appendix A). Light availability in each study reach was quantified using an Odyssey photosynthetically active radiation (PAR) logger (Dataflow Systems Ltd; Christchurch, New Zealand). We attached these loggers to rebar installed along the edge of the stream. The PAR loggers collected integrated measurements over 10-minute intervals in μmol m^{-2} s^{-1}. The PAR loggers were calibrated with a LI-COR quantum sensor (Campbell Scientific; Logan, Utah, USA). During a sensor malfunction period of 34 days between February and March 2019 in Oak Creek, in order to estimate PAR during the gap period we used a relationship between our sensor and values recorded at a nearby weather station (located 0.8 km away) during time periods with reliable data ($r^2 = 0.85$; Appendix B). There was a sensor malfunction in South Fork Mill Creek as well from March to April 2019 (total of 43 days). For this period, we used the same method to estimate PAR at our study site, using a relationship between the reliable data from our site and a solar radiation sensor from a weather station located 21 km away from our study area ($r^2 = 0.70$; Appendix B).

Dissolved oxygen (O_2, mg L^{-1}) and water temperature (degrees Celsius) were recorded every 10 minutes using MiniDOT optical dissolved oxygen and temperature loggers (Precision Measurement Engineering; Vista, California, USA). Loggers were deployed inside 1-foot long pieces of 3-inch diameter PVC pipe at the downstream end of each reach. Barometric pressure (kPa) was measured every 10 minutes with a Barologger

Edge absolute pressure sensor (Solinst; Georgetown, Ontario, Canada) in each watershed. In Oak Creek, barometric pressure was measured at the downstream end of the reach (within 10 m of the water depth and dissolved oxygen meters). In South Fork Mill Creek, the logger was installed about 1.5 km away in an adjacent sub-watershed of Mill Creek.

The downstream end of each reach was instrumented with a Levelogger Edge water level datalogger (Solinst; Georgetown, Ontario, Canada) to measure water stage every 10 minutes. These 10-minute interval water height data were compensated with the barometric pressure data, and then we calculated 10-minute interval discharge data for both reaches from depth-discharge rating curves. Discharge was calculated using the velocity area method (Dingman, 2002) by measuring velocity with a Hach FH950 Portable Velocity Meter (Hach; Loveland, Colorado, USA). The rating curve between stage height and discharge in Oak Creek (Figure 3.1a) was developed from 16 stage-discharge pairs measured between 2012 and 2017. The rating curve in South Fork Mill Creek (Figure 3.1b) was developed from 17 stage-discharge pairs measured between 2014 and 2017. In both streams, stage in meters (H) and discharge in $m^3\ s^{-1}$ (Q) were related by a power-law relationship where $Q = aH^b$. During a sensor malfunction period of 23 days between February and March 2019 in Oak Creek, we created a relationship between mean daily depths with a downstream pressure sensor 5 km away, and used this relationship to calculate depth and discharge during the gap period (Appendix B).

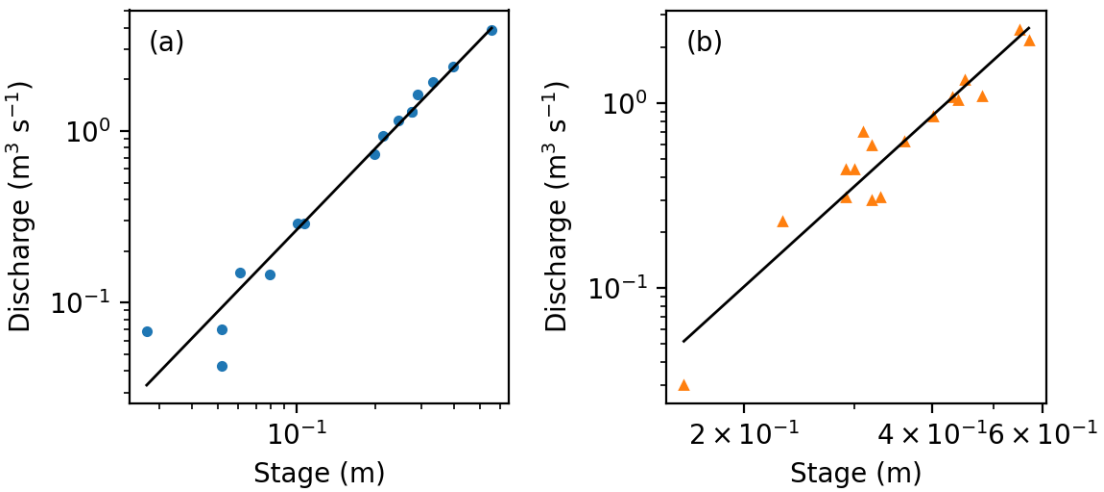

Figure 3.1 Stage-discharge rating curves for Oak Creek (a) and South Fork Mill Creek (b), fit by power-law relations ($Q = aH^b$). Measurements in Oak Creek were made between 2012 and 2017, and the best-fit line (a=10.08, b=1.58, r^2=0.96) was used to calculate 10-minute interval discharge data for the reach. Measurements in South Fork Mill Creek were made between 2014 and 2017, and the best-fit line (a=14.24, b=3.07, r^2=0.91) was used to calculate 10-minute interval discharge data for the reach.

3.1.2 Suspended Sediment Data

To measure suspended sediment concentration (SSC), we deployed Teledyne ISCO 3700 automated samplers (Teledyne ISCO; Lincoln, Nebraska, USA) at the downstream end of each reach. The samplers collected a 900 mL water sample at midnight every 24 hours for most of the rainy season (from early November to late April). In Oak Creek, sampling frequency was increased to every 3 or 6 hours during some storm events to evaluate 24-hour sampling relative to more frequent event-based sampling.

Suspended sediment concentrations of samples collected by the automated sampler were calculated by filtering the sample and weighing the inorganic sediment load on each filter. After filtering, the pre-weighed 1.5 µm glass fiber filters were dried in an oven at 105 degrees Celsius for 24 hours, then weighed. The mass of the sediment was calculated by subtracting the mass of the filter before filtering from the mass of the filter and sediment together. The mass of the water and sediment pre-filtering was calculated by subtracting the mass of the dry empty bottle from the beginning mass of the bottle, water, and sediment. After subtracting out the calculated mass of sediment, the mass of the water was converted

to a volume. With the mass of sediment and volume of water, a suspended sediment concentration in mg L^{-1} was calculated for each sample. A total of 333 samples were collected in Oak Creek – 145 in the 2018 water year and 188 in the 2019 water year – and a total of 133 samples in South Fork Mill Creek in the 2019 water year (Figure 3.2).

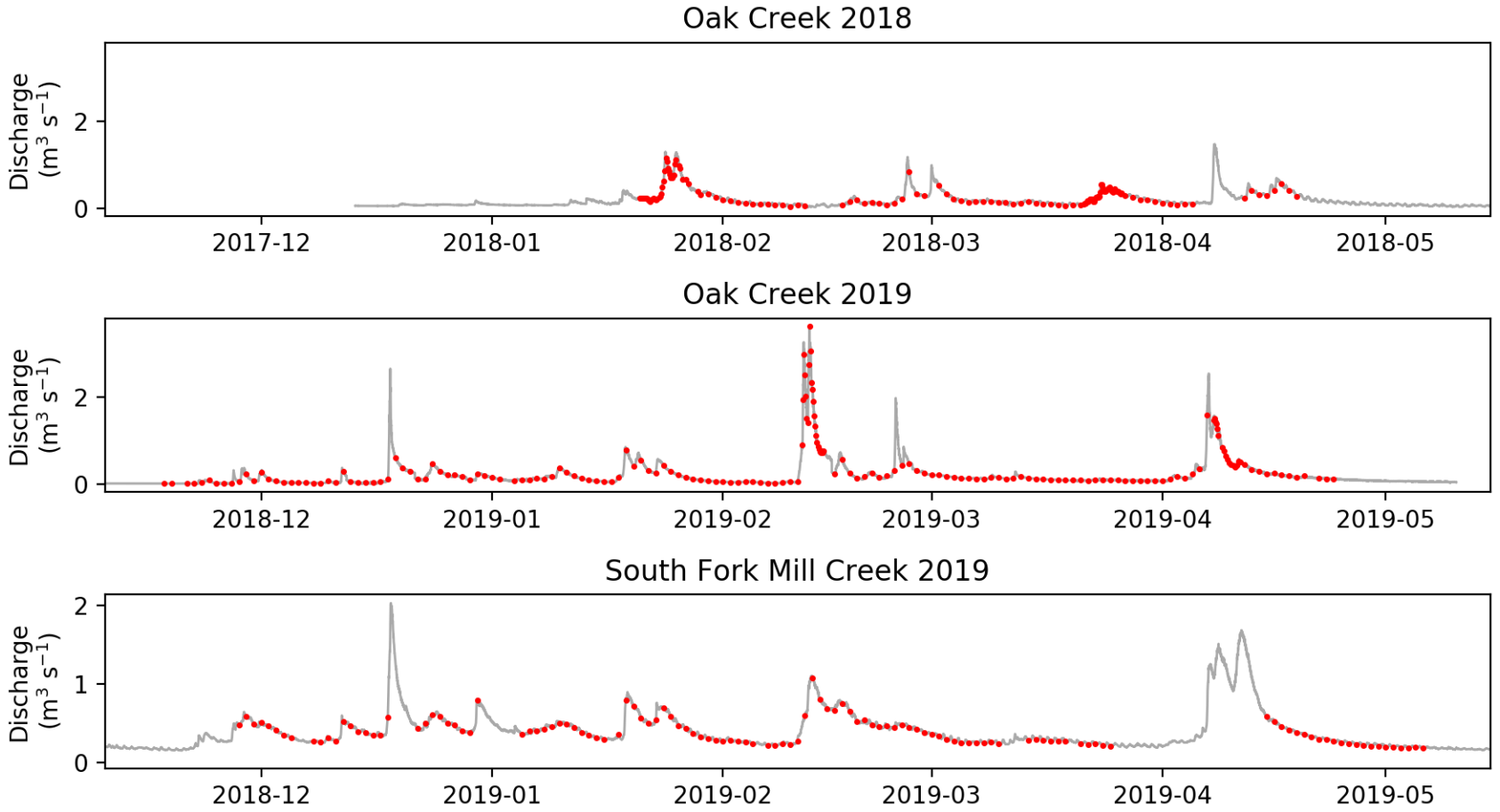

Figure 3.2 Calculated discharge and times of suspended sediment sampling in Oak Creek and South Fork Mill Creek in 2018 and 2019. Grey lines represent discharge (from 10-minute intervals), and each red dot represents a collected sample.

Daily sediment flux was calculated for both streams based on a power-law relationship between discharge (Q) and SSC, where SSC = aQ^b (Figure 3.3). With these relationships, SSC was calculated for each 10-minute interval of discharge data, which was then used to calculate the 10-minute interval sediment flux. The sediment flux fractions for each day were added together to calculate a total daily sediment flux.

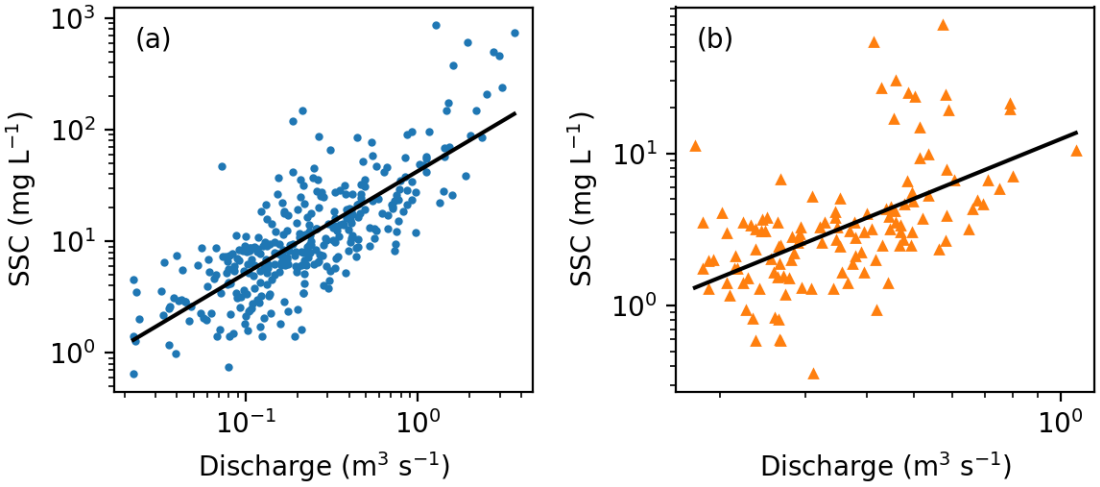

Figure 3.3 Relationship between discharge and SSC in Oak Creek (a) and South Fork Mill Creek (b). In Oak Creek, the best-fit line (a=42.64, b=0.92, r^2=0.61) was developed from 333 SSC samples. In South Fork Mill Creek, the best-fit line (a=12.40, b=1.30, r^2=0.31) was developed from 124 SSC samples.

3.2 Modeling Stream Metabolism

3.2.1 Model Parameters

We modeled stream metabolism from measurements of dissolved oxygen using a single-station open-channel method (Holtgrieve et al., 2010; Odum, 1956). We utilized the streamMetabolizer R package (https://github.com/USGS-R/streamMetabolizer), which uses inverse-modeling methods to estimate rates of GPP, ER, and K_{600} (a gas exchange rate) from diurnal O_2 curves. The model requires light (PAR, µmol m^{-2} s^{-1}), water temperature (degrees Celsius), depth (m), dissolved oxygen concentration (mg L^{-1}),

barometric pressure (millibars), and salinity (ppt). As the sites are freshwater streams, we assumed salinity was zero for both sites.

For South Fork Mill Creek, we used the binned pooling method with model defaults for estimating K_{600}. This method relates K_{600} and the discharge with piecewise linear functions, while still allowing some variation in K_{600} to be independent of discharge. This method yielded estimates that were consistent with K_{600} estimated from an SF_6 release (at a discharge of 0.29 m^3 s^{-1}) (Appendix C). This method was not successful in Oak Creek. Gas tracer releases experiments indicated that the gas exchange rates were much greater than model estimates in Oak Creek over a range of flows (see section 3.2.2). Given these high gas exchange rates, we ran the Oak Creek model without pooling K_{600} values and defined a prior distribution for K_{600} that would always have a high K_{600} value. The model required the mean and standard deviation of the lognormal distribution of K_{600} values, for which we used 5.298 (the natural logarithm of 200 day^{-1}, our chosen value of K_{600}) and 0.1 respectively.

Models were run with 3,000 Markov Chain Monte Carlo iterations (1,500 burn-in iterations). We assessed model performance using the following criteria: R-hat values less than 1.1 for daily GPP, ER, and K_{600}, and RMSE of modeled DO versus observed DO < 0.05 mg L^{-1} (~10% of daily change in observed DO) (Grace et al., 2015). We restricted our analysis of stream metabolism data to only the days on which these criteria were met (N = 196 of 405 possible dates for both streams).

3.2.2 Measuring Gas Exchange Rates

When the metabolism signal is weak due to low GPP and high gas exchange, there can be unrealistic model outputs due to equifinality, where many possible combinations of GPP, ER, and K_{600} yield the same diel curves of dissolved oxygen (Appling et al., 2018). We found this to be an issue in Oak Creek, where the small size of the stream results in turbulence that causes high gas exchange rates. Therefore, to further explore the relationship between K_{600} and discharge, we conducted three separate gas tracer releases in Oak Creek.

To calculate K_{600} using gas tracer releases, we dripped into the stream a solution that included dissolved SF_6 gas and a dissolved conservative (non-bioreactive) tracer – in

this case salt (NaCl) dissolved in stream water. We then measured the decline in sulfur hexafluoride (SF_6) concentrations relative to concentrations of the conservative tracer downstream from the addition site at the top of the reach. Samples were collected at 0m, 30m, 60m, 90m, 120m, and 150m downstream from the top of the reach. To allow the SF_6 to fully dissolve in the release water that was pumped into the stream, we added SF_6 to headspace in a solution bag 24 hours before the release. The gas-impermeable bag was half filled with water, and then SF_6 was pumped in to fill the remaining volume of the bag. After pumping began, we measured conductivity at the downstream end of the reach. Conductivity changes (driven by Na^+ and Cl^- ion concentrations) were monitored at the downstream site until the increase in conductivity at the downstream study reach remained consistent ("plateaued"). Then, starting at the downstream end, we collected water samples in triplicate at each sampling location. Water samples were collected and sealed underwater to ensure no gas loss. Gas was extracted from each water sample and the gas samples were then analyzed on an Agilent 7890A Gas Chromatograph to determine the relative decline in SF_6 concentrations downstream. The slope of the best-fit line relating SF_6 concentration to distance downstream was multiplied by the average velocity of the stream at that time of the release to determine the gas exchange coefficient for SF_6 in units of day^{-1}. This K_{SF6} value was then converted to K_{600} using the water temperature T in degrees Celsius, with the following equation (Raymond et al., 2012):

$$K_{600} = \left(\frac{600}{3255 - 217.13T + 6.837T^2 - 0.0861T^3}\right)^{-0.5} \times K_{SF6} \qquad (3.1)$$

These K_{600} values were matched with the average discharge over the period of the gas tracer release. These three data points are summarized in Table 3.1 and Appendix C.

Table 3.1 Sulfur hexafluoride release results in Oak Creek. K_{600} ranged from 206.6 day^{-1} to 289.7 day^{-1} over discharges ranging from 0.05 $m^3\ s^{-1}$ to 1.07 $m^3\ s^{-1}$.

Discharge ($m^3\ s^{-1}$)	**K_{600} (day^{-1})**
0.05	289.7
0.10	206.6
1.07	239.4

The resulting K_{600} values did not show a clear relationship with discharge but were much higher than – about double – those estimated by the metabolism model. We used these gas tracer release results to inform the definition of a high-magnitude prior distribution for the Oak Creek model discussed above. We used a value of 200 day^{-1} for the gas exchange rate coefficient. Because we found K_{600} values between 200 day^{-1} and 300 day^{-1} for a wide range of discharges (0.05 m^3 s^{-1} to 1.07 m^3 s^{-1}), we also limited the standard deviation of the lognormal distribution to 0.1.

3.3 Analysis

3.3.1 Quantile Regressions

Quantile regressions are a useful statistical tool for estimating the effects of ecological limiting factors (Cade & Noon, 2003). This method estimates relationships between variables for different portions of the distribution, as opposed to a least squares regression, which only estimates a relationship for the mean of the distribution. Due to the complexity of interactions between factors that affect organisms, it can be more meaningful to focus on the quantiles near the maximum response, where the limiting factor is driving the response (Cade & Noon, 2003).

We calculated the slope of the 80^{th} quantile regression between GPP and two physical attributes: maximum daily discharge and daily suspended sediment flux. We also calculated these slopes between the P/R ratio and the two physical attributes. The 80^{th} quantile was chosen because it is the upper-most quantile before sampling variation begins to increase (Cade et al., 1999) (Appendix D). The slope was calculated first for the relationship between the physical attributes the day of the modeled metabolic rates and the metabolic rates. Because we are evaluating a lagged effect of bedload movement events on stream metabolism in addition to effects during the event itself, we also calculated the regression slopes with a lag of between 1 to 18 days between the physical attribute and the metabolic rates. The series of slopes for each combination were plotted over time to explore the legacy effects of elevated discharge and suspended sediment flux on GPP and the P/R ratio.

3.3.2 Storm Before-After Analysis

We explored differences in GPP and ER pre- and post-storm for the three largest flows in the 2019 study period. These flows generally followed the same time periods in Oak Creek and South Fork Mill Creek, but had different relative magnitudes of increased discharge in the two systems. For each of the three storms, we established the peak discharge and an end date for the flood, chosen as the date when flows returned to pre-storm levels. We binned values of GPP and ER from between 1–12 days before the peak of the storm for a 'before' category, and then binned values between 1–3, 4–6, 7–9, 10–12, and 13–15 days after the end of the storm. In each 'after' category, the box plots had between 1–3 data points depending on availability of modeled data during that time period. In cases where only a line was plotted, there was only one data point modeled during that three-day period. From these binned data, we compared patterns in disturbance and recovery. We also calculated the percent decrease in both GPP and ER for each storm between the pre-storm period and the period 1-3 days after the storm.

3.3.3 Metabolic Fingerprint

Patterns in stream metabolism can be compared between streams through a metabolic a kernel density plot of daily estimates of GPP and ER in a stream, creating what is known as a metabolic fingerprint (Bernhardt et al., 2018). The 1:1 line is also plotted on the figure. Points that fall above the line represent autotrophy in the stream, while points below the line represent heterotrophy. It is expected that the area covered by the fingerprint would represent the factors affecting metabolic rates: an expanded area would result from increased light, nutrients, or temperature, while physical disturbances restrict the area (Bernhardt et al., 2018).

4 Results

4.1 Calculation and Modeling Results

4.1.1 Metabolism Modeling

Our analysis yielded successful models of gross primary production (GPP), ecosystem respiration (ER), and K_{600} for 95 days in South Fork Mill Creek between December 2018 and April 2019, and for 101 days in Oak Creek between December 2017 and April 2018 and between December 2018 and April 2019 (Appendix E). Modeled K_{600} in Oak Creek ranged from 73.6 to 330.5 d^{-1}, and in South Fork Mill Creek ranged from 18.0 to 38.9 d^{-1} (Figure 4.1). Modeled GPP and ER had larger ranges in Oak Creek than South Fork Mill Creek; GPP ranged from 0.0 to 0.8 g O_2 m^{-2} d^{-1}, while the modeled ER ranged from -12.6 to -5.5 g O_2 m^{-2} d^{-1} (Figures 4.2, 4.3). Modeled GPP in South Fork Mill Creek ranged from 0.0 to 0.7 g O_2 m^{-2} d^{-1}, while the modeled ER ranged from -8.9 to -2.9 g O_2 m^{-2} d^{-1} (Figure 4.4). The 2019 winter-spring period had higher magnitude high flow events than in 2018. In Oak Creek, the highest flow during the 2018 study period was $0.43Q_{bf}$, while the highest flow was $1.06Q_{bf}$ in the 2019 study period. In South Fork Mill Creek, the highest flow was $0.81Q_{bf}$.

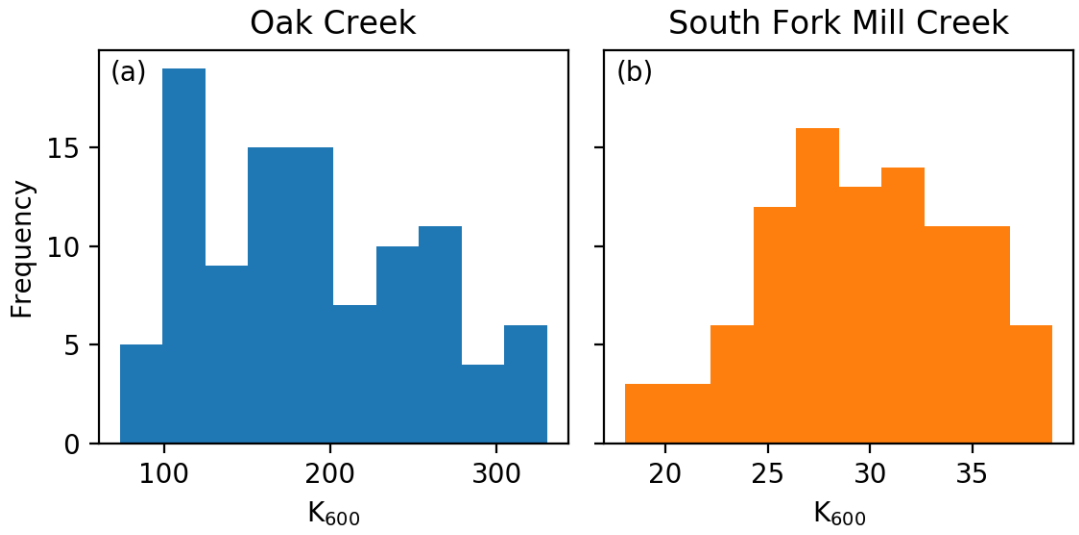

Figure 4.1 Histograms of modeled K_{600} values in Oak Creek (a) and South Fork Mill Creek (b). K_{600} ranged from 73.6 d^{-1} to 330.5 d^{-1} in Oak Creek and from 18.0 d^{-1} to 38.9 d^{-1} in South Fork Mill Creek.

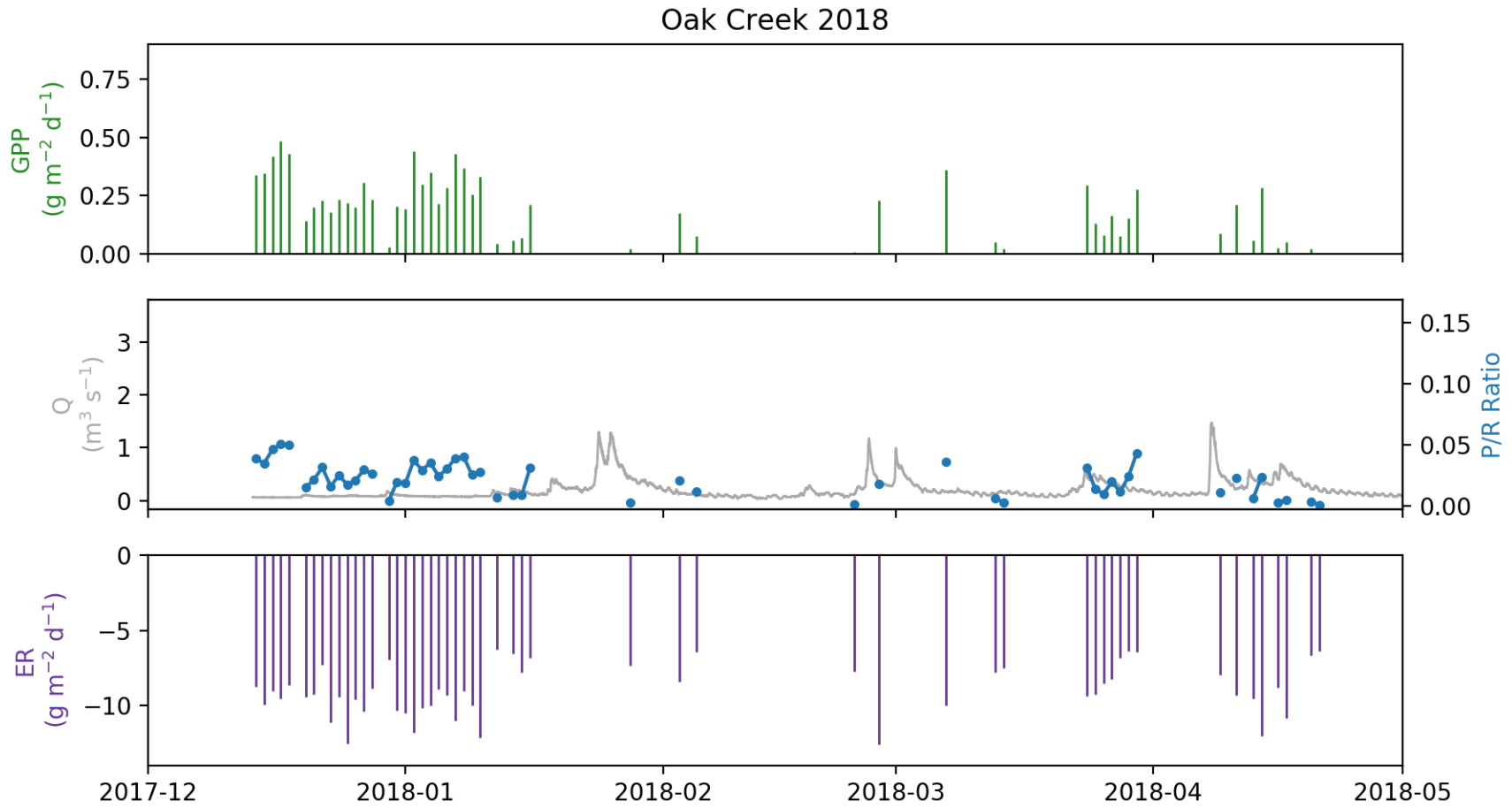

Figure 4.2 Modeled GPP and ER in Oak Creek in the 2018 water year. GPP ranged from 0.0 g m^{-2} d^{-1} to 0.5 g m^{-2} d^{-1} while ER ranged from -12.6 g m^{-2} d^{-1} to -6.3 g m^{-2} d^{-1}. P/R ratio is shown in the middle plot. The highest discharge (April) was $0.43Q_{bf}$.

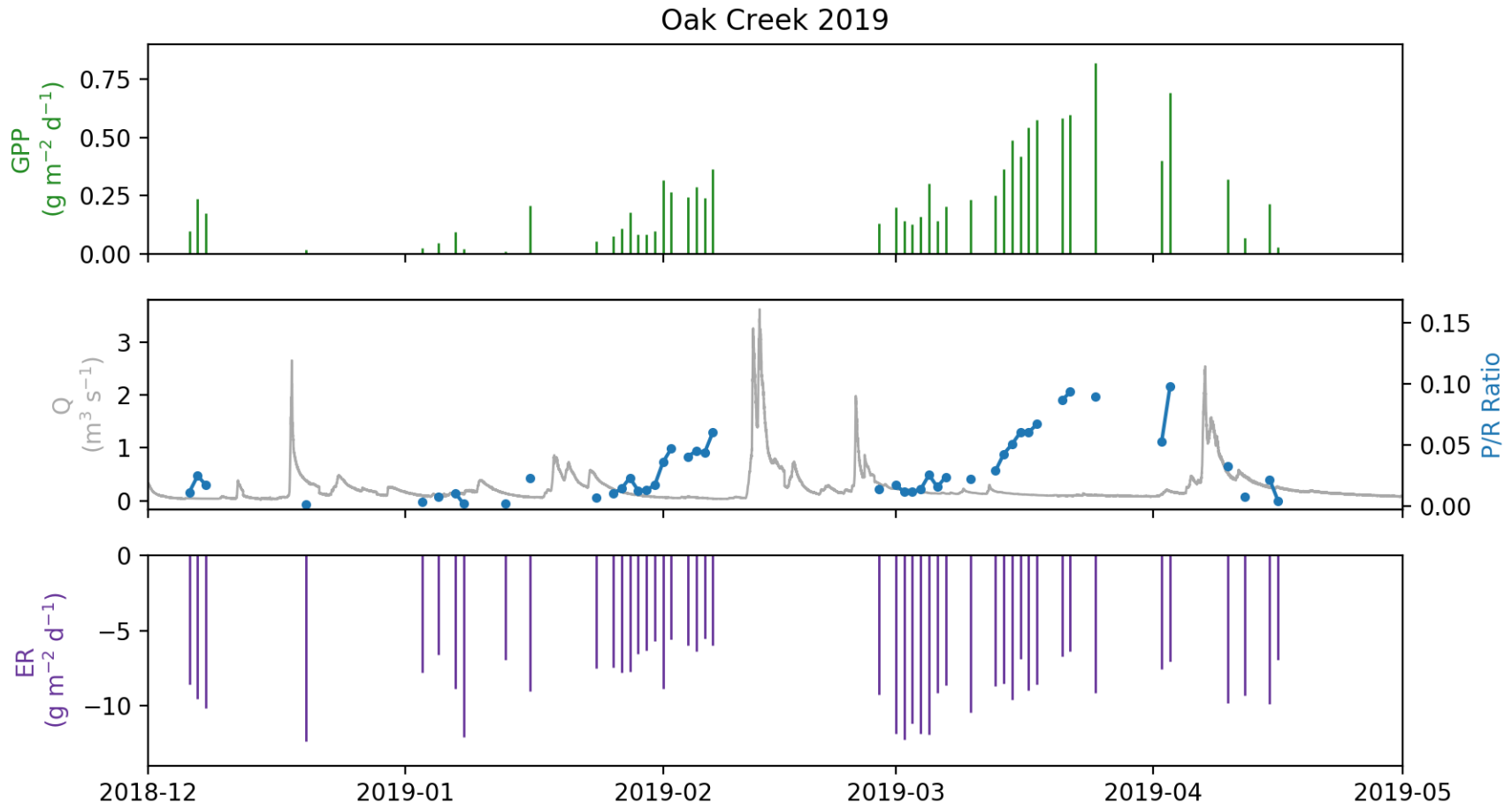

Figure 4.3 Modeled GPP and ER in Oak Creek in the 2019 water year. GPP ranged from 0.0 g m^{-2} d^{-1} to 0.8 g m^{-2} d^{-1} while ER ranged from -12.4 g m^{-2} d^{-1} to -5.5 g m^{-2} d^{-1}. P/R ratio is shown in the middle plot. The highest discharge (February) was $1.06Q_{bf}$.

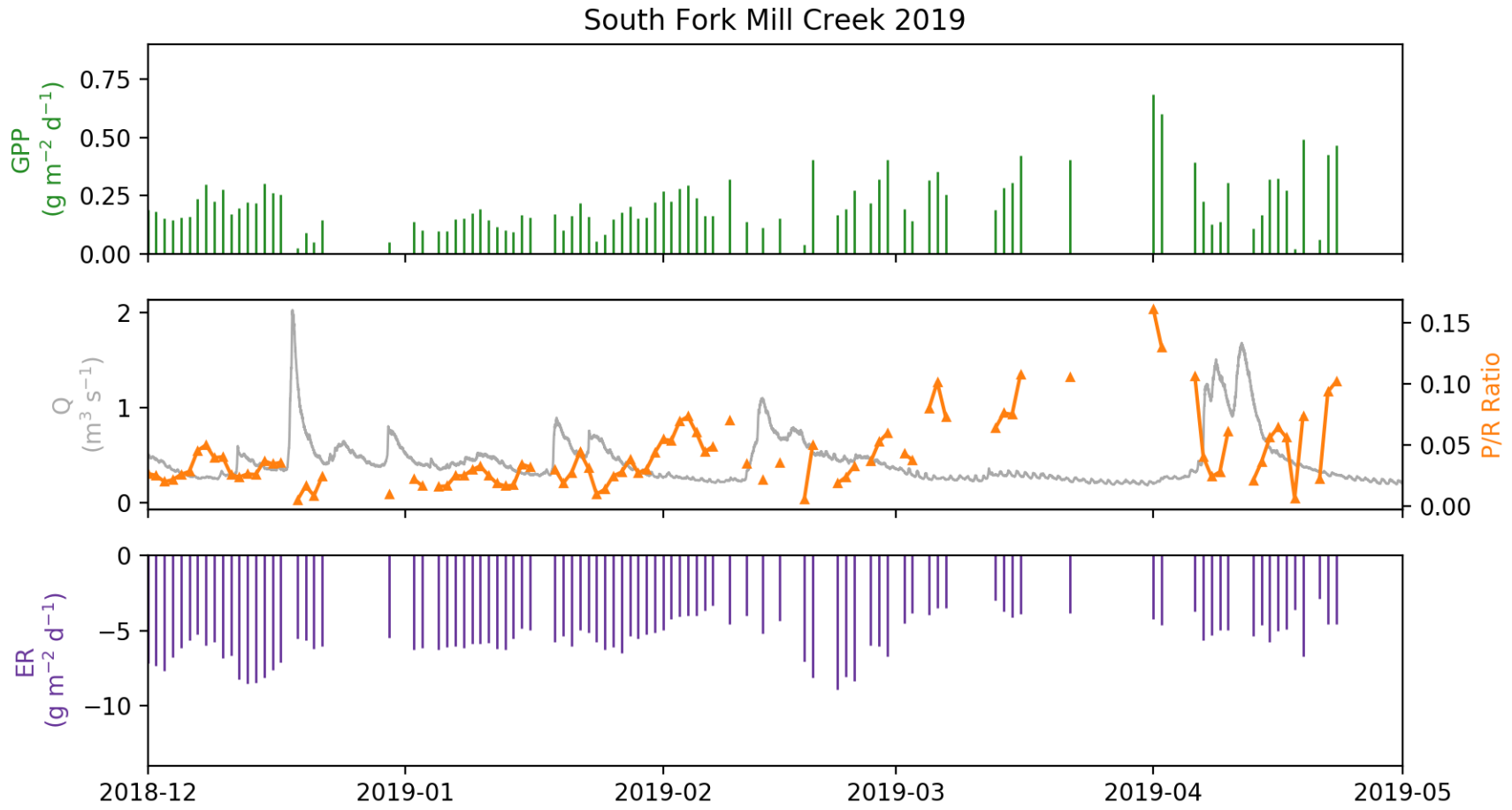

Figure 4.4 Modeled GPP and ER in South Fork Mill Creek in the 2019 water year. GPP ranged from 0.0 g m^{-2} d^{-1} to 0.7 g m^{-2} d^{-1} while ER ranged from -8.9 g m^{-2} d^{-1} to -2.9 g m^{-2} d^{-1}. P/R ratio is shown in the middle plot. The highest discharge (December) was $0.81Q_{bf}$.

4.1.2 Suspended Sediment Analysis

The SSC of samples collected from Oak Creek ranged from 0.65 mg L^{-1} to 876.08 mg L^{-1}, while the range of SSC of samples collected from South Fork Mill Creek was substantially lower (from 0.35 mg L^{-1} to 70.21 mg L^{-1}). Both streams showed an increase in suspended sediment with discharge, but for similar levels of discharge, South Fork Mill Creek generally had a lower suspended sediment flux (Figure 4.5).

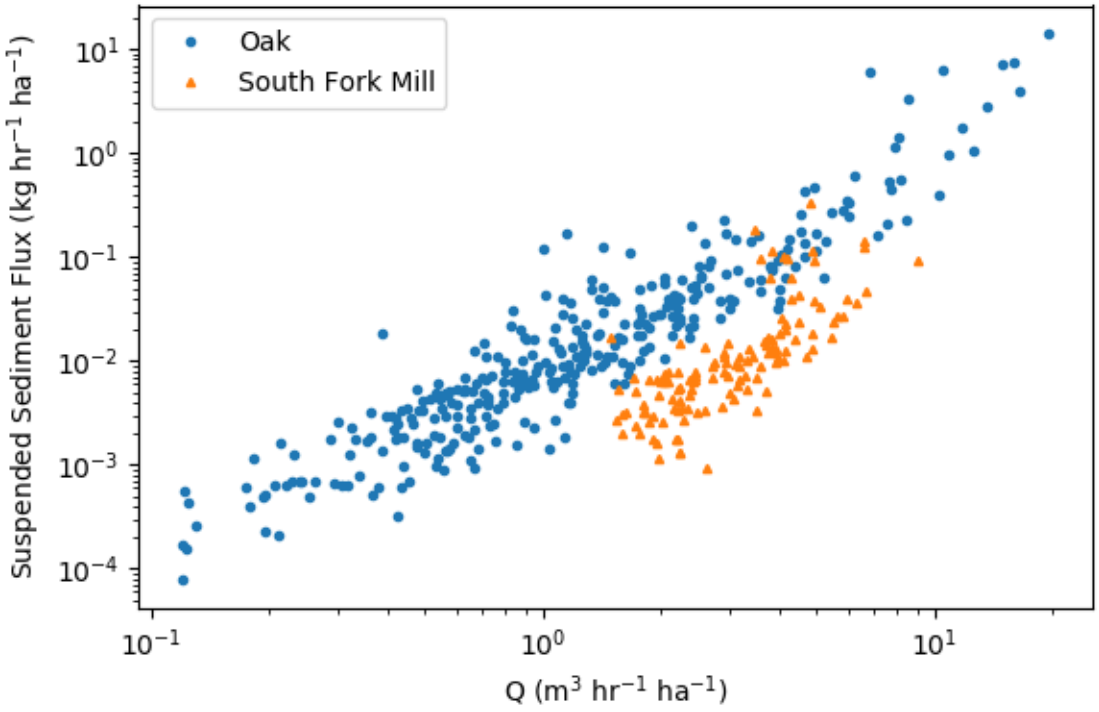

Figure 4.5 Suspended sediment flux and discharge from samples collected in Oak Creek and South Fork Mill Creek. Oak Creek generally showed more suspended sediment flux than South Fork Mill Creek at similar levels of discharge.

4.2 Relationships between Discharge, Suspended Sediment Flux, and Ecosystem Metrics

In both Oak Creek and South Fork Mill Creek, the maximum observed rate of gross primary production (GPP) declined as both stream discharge and stream suspended sediment flux increased (Figure 4.6a, 4.6b). This is illustrated by negative slopes of the 80th quantile regressions between both GPP and maximum discharge on that day, and between daily GPP and the total estimated sediment flux through each reach during that

day. Slopes of these relationships were similar in Oak Creek and South Fork Mill Creek. The slope of the 80th quantile regression in Oak Creek was -0.24, while in South Fork Mill Creek it was -0.29. Similarly, the relationship between GPP and sediment flux over the same time period had a slope of -0.11 in Oak Creek and -0.13 in South Fork Mill Creek.

We also investigated the legacy of elevated discharge and sediment flux through a quantile regression analysis with maximum discharge and suspended sediment flux for the days before GPP was modeled (Figure 4.6c, 4.6d). Maximum discharge had less of a legacy effect on GPP in South Fork Mill Creek than in Oak Creek. The slope of the quantile regression approached 0 (indicating no relationship between GPP and maximum discharge a given number of days before) after only a few days in South Fork Mill Creek (Figure 4.6c). In contrast, in Oak Creek it took 17 days before the slope of the 80th quantile regression between maximum discharge and GPP reached 0 (Figure 4.6c). Suspended sediment flux showed a similar trajectory – the slope of the regression in South Fork Mill Creek approached 0 around 10 days before the slope in Oak Creek did (Figure 4.6d).

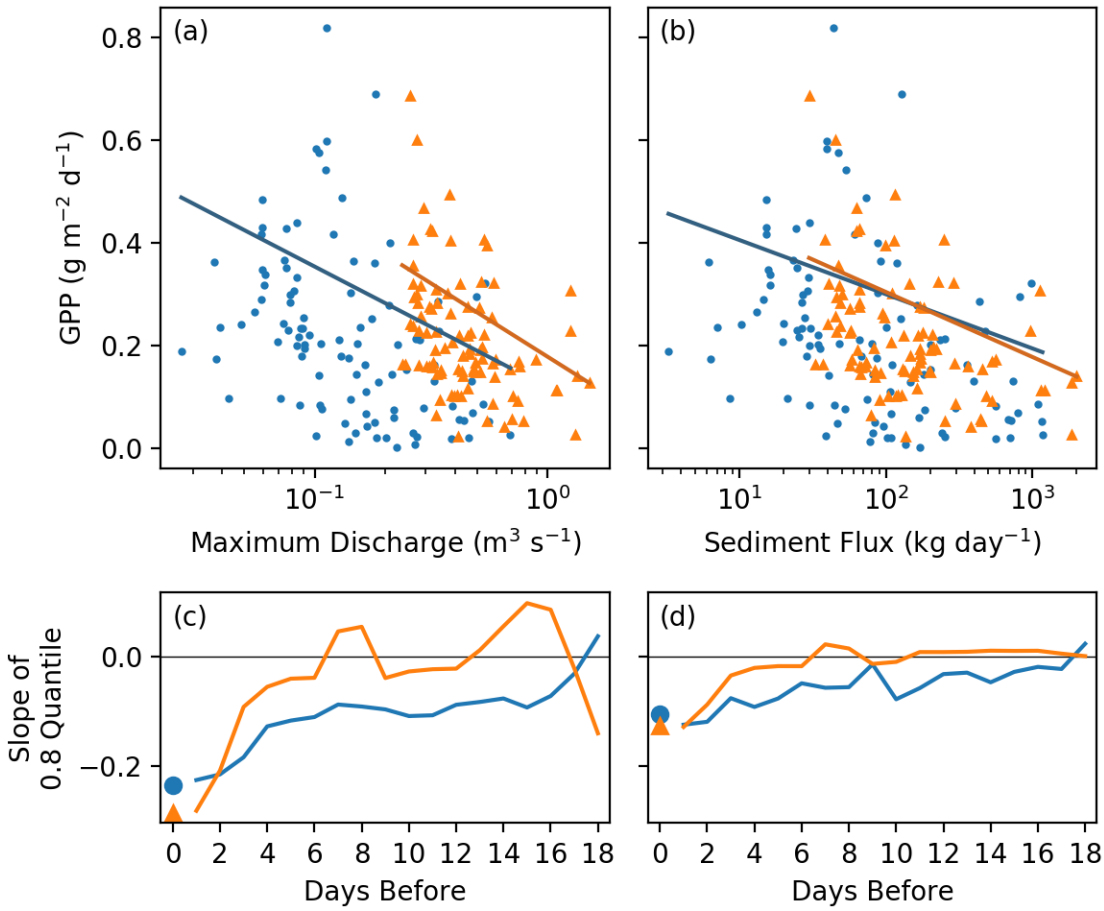

Figure 4.6 Results of 80th quantile regressions between gross primary productivity (GPP) and same-day maximum discharge (a) and between GPP and same-day sediment flux (b). The bottom panels show the slopes of the 80th quantile regressions between GPP and the physical variable (maximum discharge (c) or daily sediment flux (d)) *x* days before the day GPP was modeled. A slope of 0 indicates no controlling effect by the physical attribute.

The P/R ratio in both streams declined with increasing discharge and suspended sediment flux (Figure 4.7a, 4.7b). The slope of the 80th quantile regression with maximum discharge in Oak Creek was -0.04, while the slope was -0.07 in South Fork Mill Creek. The same-day suspended sediment flux relationship slope of the 80th quantile was -0.02 in Oak Creek and -0.03 in South Fork Mill Creek. In both cases, while the same-day relationships in South Fork Mill Creek had steeper slopes than in Oak Creek, the legacy of the change in P/R ratio for both streams declined by around 10 days (Figure 4.7c, 4.7d).

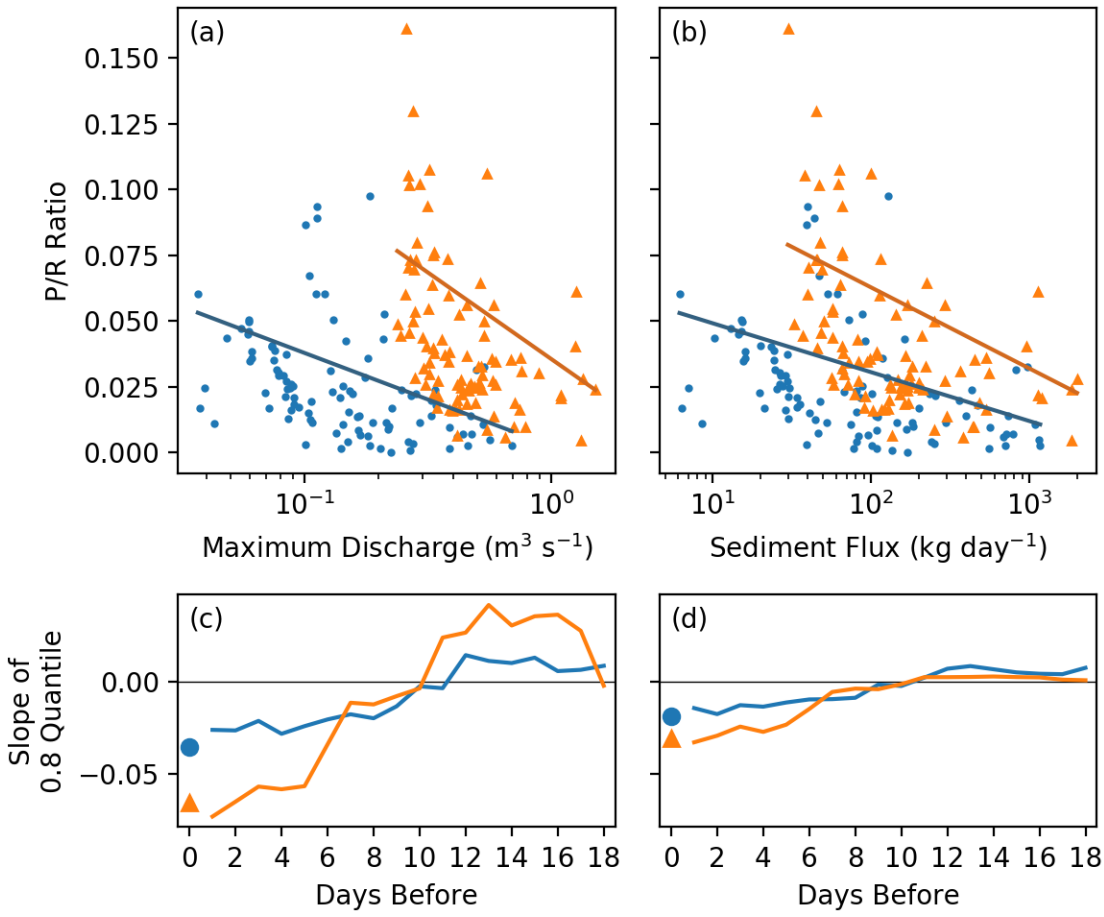

Figure 4.7 Results of 80th quantile regressions between the P/R ratio and same-day maximum discharge (a) and between the P/R ratio and same-day sediment flux (b). The bottom panels show the slopes of the 80th quantile regressions between the P/R ratio and the physical variable (maximum discharge (c) or daily sediment flux (d)) *x* days before the day the P/R ratio was calculated. A slope of 0 indicates no controlling effect by the physical attribute.

4.3 Evaluating Individual Storm Effects on GPP and ER

For the three largest storms in 2019 (Table 4.1), we observed a decrease in GPP from the days before the storm to the days after the end of the storm (Figure 4.8). The decrease in mean GPP between before the storm and 1–6 days after ranged from 36.9% to 81.0% in Oak Creek and from -3.8% (a slight increase) to 54.3% in South Fork Mill Creek (Table 4.1). Over the course of the season, the before-storm GPP increased in both streams, with the December storm having the lowest preceding GPP and the April storm having the

highest preceding GPP. The GPP in Oak Creek declined by over 80% following the April storm, which had a peak flow of 75% of bankfull (Table 4.1). In South Fork Mill Creek, the April and December storms had comparable impacts on GPP with about a 55% decline in GPP following storms that were 81% and 67% of bankfull for the December and April storms, respectively. The GPP recovered more quickly in South Fork Mill Creek than in Oak Creek for all three storms (Figure 4.8).

Table 4.1 Storm characteristics for the three largest storms in the 2019 water year. The storm with the highest peak in Oak Creek ($1.06Q_{bf}$) was in February, while the storm with the highest peak in South Fork Mill Creek ($0.81Q_{bf}$) was in December. For the % Drop values, negative percentages represent an increase in rates of GPP and ER.

Reach	% Drop in GPP (1–6 days after)	% Drop in ER (1–6 days after)	Peak Date	End Date	Peak Discharge (Q_i/Q_{bf})
Oak	67.8%	2.7%	12/18/18	1/4/19	0.78
	36.9%	-69.7%	2/12/19	3/1/19	1.06
	81.0%	-19.3%	4/7/19	4/11/19	0.75
South Fork Mill	53.6%	-3.4%	12/18/18	1/2/19	0.81
	-3.8%	2.1%	2/12/19	3/1/19	0.44
	54.3%	-0.4%	4/11/19	4/17/19	0.67

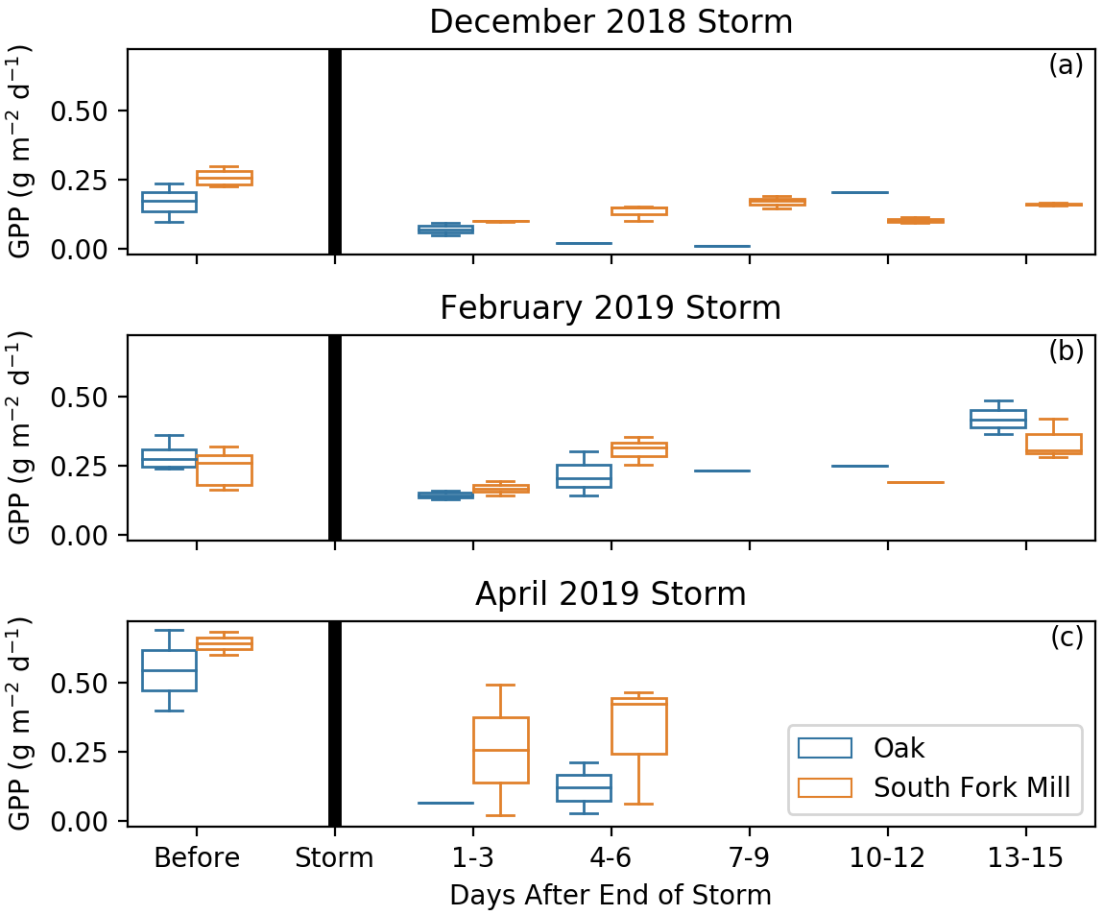

Figure 4.8 GPP before and after the three largest storm events in the 2019 water year. The 'before' category included data from 1–12 days before the peak of the storm. The 'after' category included data from after the end of the storm – when flows returned to pre-storm levels. Over the course of the study period, the pre-storm GPP rose, resulting in a larger drop due to the storm. In all three cases, South Fork Mill Creek appeared to rise more rapidly after the storms.

The ER responses to the storm events in December, February, and April of 2019 differed from the GPP responses in Oak Creek and South Fork Mill Creek. The December storm had minimal effects on mean ER in Oak Creek (Table 4.1), and following the storms in both February and April, post-storm mean ER increased (became more negative), which contrasts with the declines observed in mean GPP at this site after these storms. In South Fork Mill Creek, ER remained relatively consistent before and after the storms (both short and long-term) with no more than 3.4% change after any of the storms (Table 4.1, Figure 4.9).

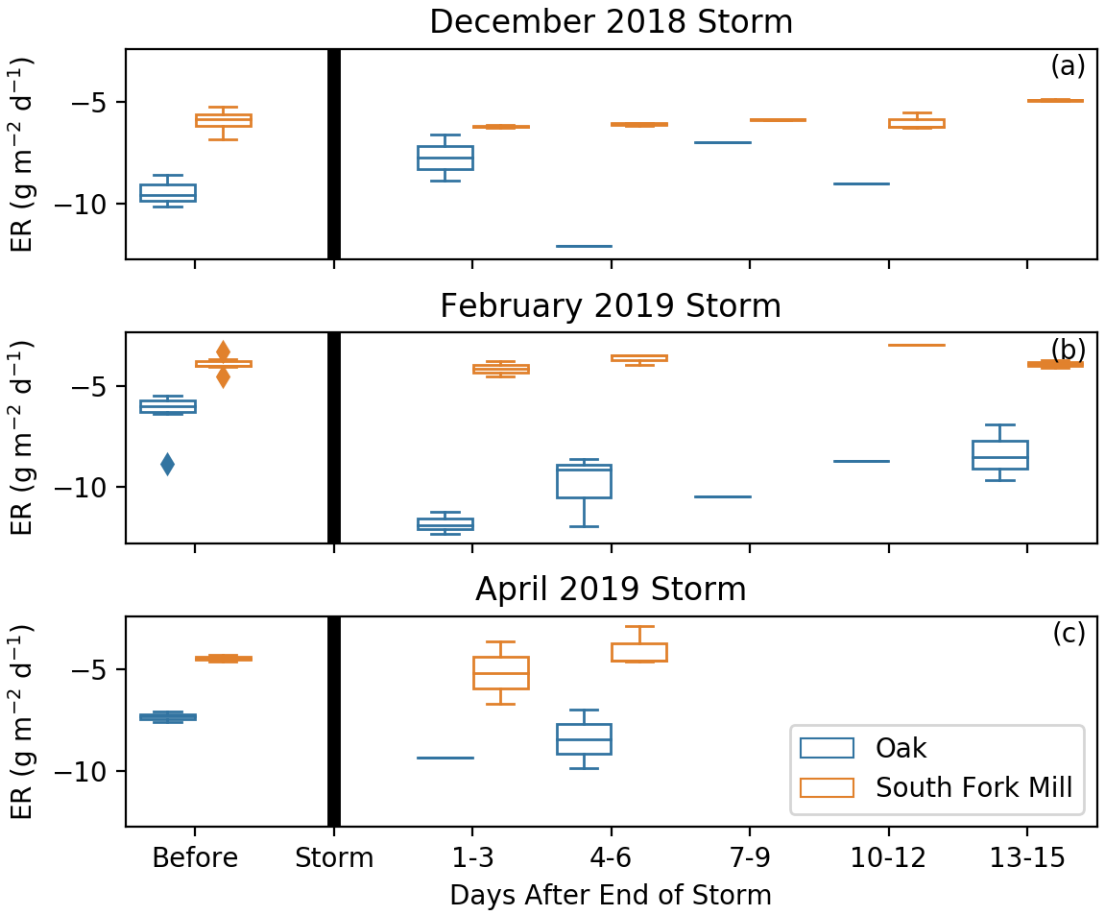

Figure 4.9 ER before and after the three largest storm events in the 2019 water year. The 'before' category included data from 1–12 days before the peak of the storm. The 'after' category included data from after the end of the storm – when flows returned to pre-storm levels.

4.4 Metabolic Regimes

The metabolic regime of the study streams through the winter and early spring were somewhat comparable between sites when assessing days in which we had model estimates of GPP and ER in both streams (total of 38 days). Both streams are highly heterotrophic during the winter-spring seasons, with much more respiration occurring than production (Figure 4.10). The range of GPP values were similar, but Oak Creek generally had more respiration than South Fork Mill Creek (Figure 4.10a). Ecosystem respiration over the 38 days with overlapping data was almost twice as variable in Oak Creek as in South Fork Mill Creek (σ = 1.95 g m^{-2} d^{-1} for Oak Creek and 1.02 g m^{-2} d^{-1} for South Fork Mill Creek).

The variability in GPP was comparable between the two streams (σ = 0.14 g m^{-2} d^{-1} for Oak Creek, σ = 0.11 g m^{-2} d^{-1} for South Fork Mill Creek). During the 38 days when both streams had data, the cumulative ER in Oak Creek was slightly less than two times that of South Fork Mill Creek (-316.38 g m^{-2} d^{-1} for Oak Creek and -186.46 g m^{-2} d^{-1} for South Fork Mill Creek; Figure 4.10b). The cumulative GPP in Oak Creek was 7.45 g m^{-2} d^{-1}, while the cumulative GPP in South Fork Mill Creek was greater at 8.76 g m^{-2} d^{-1}.

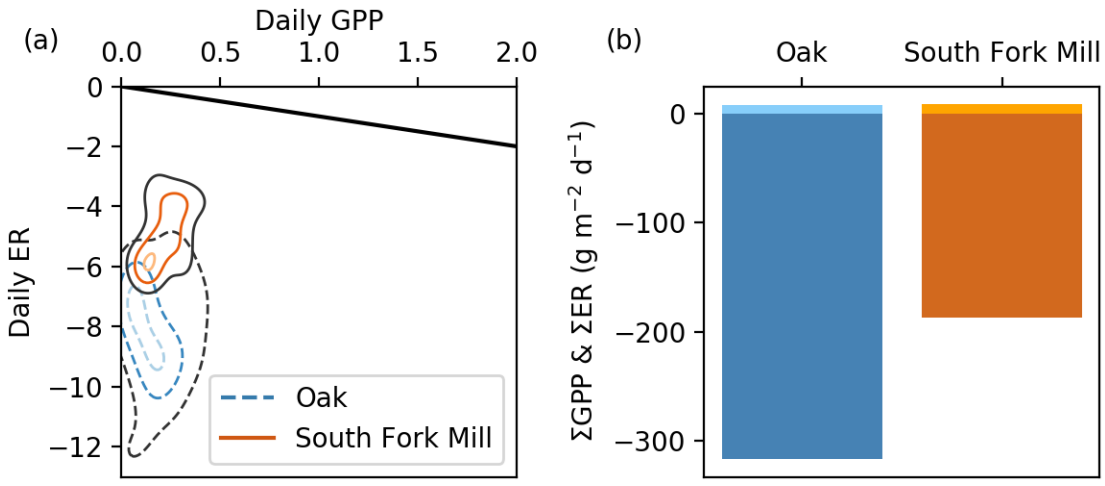

Figure 4.10 (a) Kernel density estimate plot of modeled GPP and ER in Oak Creek (blue) and South Fork Mill Creek (orange) on days when both streams had modeled estimates (38 days). The 1:1 line is shown with a solid black line. (b) Cumulative GPP (light blue, light orange) and ER (dark blue, dark orange) over the days in which metabolic rates were modeled in both sites. Over these 38 days, the cumulative GPP in Oak Creek was 7.45 g m^{-2} d^{-1}, and in South Fork Mill Creek was 8.76 g m^{-2} d^{-1}. The cumulative ER in Oak Creek was -316.38 g m^{-2} d^{-1}, and in South Fork Mill Creek was -186.46 g m^{-2} d^{-1}.

4.5 Light and Temperature

Differences in water temperature and light availability could lead to differences in both GPP and ER in streams that would confound conclusions about the influence of physical processes in this study, but overall light and temperature were largely comparable along the two study reaches. Average water temperature during the study period ranged from 3.89 degrees C to 11.66 degrees C in Oak Creek, and from 4.88 degrees C to 10.55 degrees C in South Fork Mill Creek. Daily PAR ranged from 0.64 mol m^{-2} to 14.93 mol m^{-2} in Oak Creek, and from 0.40 mol m^{-2} to 16.48 mol m^{-2} in South Fork Mill Creek. Neither

stream had a strong or significant relationship between light or temperature and GPP during our study period ($r^2 < 0.003$, $p > 0.5$) (Figure 4.11a, 4.11b). In Oak Creek, neither temperature nor PAR show a significant relationship with ER ($r^2 < 0.05$, $p > 0.05$). Similarly, there is no significant relationship between ER and temperature in South Fork Mill Creek ($r^2 < 0.03$, $p > 0.1$) (Figure 4.11c, 4.11d). There is a relationship between PAR and ER at this site, but it only explains 13% of the variance in the data ($r^2 = 0.13$, $p < 0.001$) (Figure 4.11d).

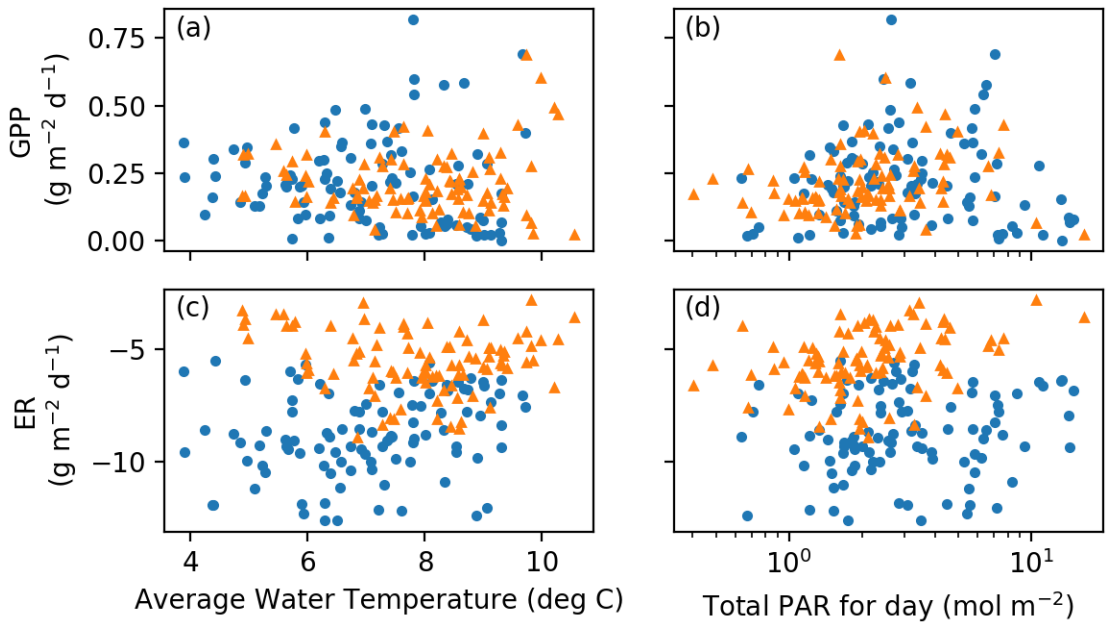

Figure 4.11 Modeled GPP and ER relative to average daily water temperature (a, c) and cumulative daily PAR (b, d). Oak Creek is represented by blue circles, and South Fork Mill Creek by orange triangles. There were no significant relationships between these factors and GPP or ER during our study period.

5 Discussion

The goal of this study was to compare patterns in stream metabolism between streams with contrasting underlying lithologies. Contrary to our expectations, South Fork Mill Creek, the sandstone basin, showed less of a response to disturbance from increased flows and suspended sediment fluxes than Oak Creek, the basalt basin. The rates of GPP decreased in both streams but had a smaller proportional decrease in South Fork Mill Creek than in Oak Creek. Both streams were heterotrophic throughout the study period and had low rates of productivity, but overall P/R ratio variation was driven by rates of ER. Rates of ER in South Fork Mill Creek did not change from pre- to post-storm, while rates of ER in Oak Creek increased.

Physical disturbances in a stream can frequently impact ecosystems process during an event, but if recovery is rapid, the disturbance may have little overall effect on the ecosystem (e.g. Roberts et al., 2007). In contrast, if recovery is prolonged, the disturbance can be key in structuring the ecosystem (e.g. Segura et al., 2011). We explored legacy effects of storm events in these two systems through a comparison of pre- and post-storm means and a quantile regression analysis. The quantile regression analysis provides information on the storm event as one of many potential limiting effects on GPP, ER, or P/R ratios. A more negative slope for the upper quantile in this study represents a larger decline in the maximum (upper 80% of the distribution in this study) value of a metric (GPP, ER, or P/R) in response to a storm event. If the quantile slope is 0, the disturbance event has no impact on the upper values of GPP, ER, or P/R and we conclude that it is not a limiting factor. We consistently saw the steepest 80% quantile slope during or shortly after a storm, indicating maximum effect during and shortly after the event. Over time, the effect of the storm event on GPP and P/R declined, reflecting recovery of these processes from the storm disturbance, with the time (in days) that it takes to return to a slope of zero in the 80% quantile reflecting the overall recovery time. From this analysis, we can see that while the initial influence of flow on GPP is larger (steeper slope) in Mill Creek, the system recovered more quickly with the transition to a slope of zero in the 80% quantile within 6 days, in contrast to Oak creek where GPP took over two weeks to recover based on this analysis. We compared these quantile regression legacies for GPP and P/R ratios.

When considering specific storm events, as we expected, GPP decreased in both streams following a storm event. However, the magnitude of the disturbance was smaller in South Fork Mill Creek than in Oak Creek. Similarly to the result of Roberts et al. (2007) in a forested headwater stream, we found that the magnitude of the disturbance did not appear to be related only to the size of the storm, but also to pre-storm conditions and the time of the season in which the storm took place. Storms had a larger effect in April in both of our streams, when pre-storm rates of GPP were higher, resulting in a larger proportional change in GPP. In both streams our comparison of GPP rates before and after storms and in our analysis of legacy responses, South Fork Mill Creek showed a faster recovery of GPP than Oak Creek. One possible explanation is that an increased concentration of clay particles in Oak Creek results in the attenuation of light to the stream bed for a longer period after storms than in South Fork Mill Creek, which continues to restrict production (Hall Jr. et al., 2015; O'Connor et al., 2012). Although we did not measure turbidity, we did observe lower clarity in Oak Creek during the winter and spring. Another possibility is that differences in the algal community and disturbance history between the two streams drive different patterns of recovery after disturbance. Indeed, a previous study in Oak Creek reported that benthic algae recovered faster in areas that are more frequently disturbed (Katz et al., 2018) and attribute this to possible differences in the algal community composition.

Rates of ER are often driven by autotroph respiration, so they often correlate with rates of GPP, although when allochthonous inputs are high, these processes can be decoupled. We initially expected that like GPP, ER would be disturbed in both streams post-storm. However, the ER legacy differed between the two streams, as storms had no effect on the magnitude of ER in South Fork Mill Creek, while the magnitude of ER consistently increased in Oak Creek post-storm. Changes in ER are the result of a combination of processes, including disturbance by flows and bed movement, as well as changes to external inputs of dissolved organic carbon (DOC). Storms result in an influx of DOC from the area surrounding the stream, which can temporarily increase ER (Beaulieu et al., 2013; Webster & Meyer, 1997) by providing a food source to consumers in the system. Decreases in ER can result from increased flow velocities and bed movement disrupting benthic organisms (Uehlinger, 2000, 2006) and decreasing their metabolic rates.

Bed movement can displace not only primary producers on the surface of the stream bed, but also other micro- and macroscopic organisms that reside deeper within the sediment of the channel bed (Naegeli & Uehlinger, 1997). Both systems in our study are forested with organic material that can enter the stream during the winter, and so likely to receive inputs of DOC (Raymond & Saiers, 2010) which would increase ER through use by heterotrophic microbes during and in the period soon post-storm. This is seen in Oak Creek. In South Fork Mill Creek, we did not see the same increase in ER during the storm; we suggest that this could be due to a lack of DOC inputs, or disturbances that reached deeper into the stream bed and therefore scoured not only substrates that support benthic autotrophs, but also heterotrophic microbes that would be able to utilize the increases in DOC. Oak Creek has a larger, less variable grain size distribution, while South Fork Mill Creek has a smaller median grain size and more patchy bed substrate. Several of the patches in South Fork Mill Creek are significantly finer than the median grain size, and it is likely the material in these patches is transported more frequently and to a further depth in the stream bed. As a result, a larger area of the bed in South Fork Mill Creek could be disturbed more frequently and more deeply below the bed surface. Given the substrate size distribution in Oak Creek, higher flows relative to those in South Fork Mill Creek would be required to break the surface armoring and disturb deeper into the bed (Parker & Klingeman, 1982). Disturbance through abrasion, increased flow velocities, and the blockage of light to the bed will disturb respiration of primary producers on the bed surface, but deeper disturbances can displace organisms other than photoautotrophs, which respire but do not use light for primary production. This could explain the increases of ER we observed in Oak Creek compared to the lack of change of ER in South Fork Mill Creek.

When GPP and ER were integrated into the P/R ratio, both streams had a similar recovery period that lasted for at least a week. The quantile regression analysis showed a lower P/R ratio with increasing maximum discharge and suspended sediment flux, with a steeper slope in South Fork Mill Creek than Oak Creek for same-day physical attributes, indicating a more limiting effect in South Fork Mill Creek. We observed that although South Fork Mill Creek had a higher magnitude slope initially, the analyses in both streams returned to a slope of 0 in around 10 days indicating overall very similar productivity to respiration ratio recovery periods.

In South Fork Mill Creek, we observed generally lower suspended sediment concentrations overall than in Oak Creek. This result could be due to differences in the breakdown of the rock types that underlie the basins. Sandstone is more friable (O'Connor et al., 2014), but weathers into sand and does not get much smaller (McBride & Picard, 1987). In contrast, while basalt is a harder rock (O'Connor et al., 2014), the products of basalt weathering are clays (Glasmann & Simonson, 1985). Clays are much finer and more readily mobilized, possibly resulting in the higher suspended sediment concentrations in Oak Creek. Sand grains in South Fork Mill Creek are likely still transported, but possibly as bed load rather than suspended sediment load.

Light, temperature, and nutrients are all resources that can affect GPP and ER, but their relative importance is influenced by their availability relative to other limiting factors (Bernhardt et al., 2018). We found that during our study period, neither light nor temperature had a significant relationship with GPP or ER; this result is likely due to low winter light, low temperature conditions, and a higher relevance of other factors such as increased flow and abrasion (Blaszczak et al., 2019). While there are several controls on metabolic rates in streams, physical disturbances represent a different kind of control, an abiotic resetting mechanism rather than a driver of biotic processes. Lithology is affecting stream metabolism in our paired streams, but not in the way we initially expected. Differing P/R ratios were driven by changes in ER rather than changes in GPP. While we acknowledge the narrow scope of inference in comparing two streams in the Oregon Coast Range, we provide an important piece of work exploring the effects of sediment mobility and disturbance on metabolic processes in small mountain streams. Further improving our understanding the effects of storms on metabolic processes in natural gravel-bed streams will require more in-depth comparisons with other lithologies and a three-dimensional view of the stream bed, as storms affect organisms both on the surface of the bed and organisms deeper within the substrate.

6 Conclusion

We investigated patterns in stream metabolism in the winter-spring season in two basins with contrasting lithology in the Oregon Coast Range. Our results indicated variations in patterns of response and recovery between the two streams. Rates of GPP decreased post-storm in both streams, but the magnitude of disturbance was less in South Fork Mill Creek than in Oak Creek, possibly due to light attenuation by clay particles in Oak Creek or differences in algal community. Post-storm, South Fork Mill Creek showed a faster recovery of GPP than Oak Creek. Rates of GPP and ER were decoupled during our study period; while GPP decreased post-storm in both streams, ER did not change in South Fork Mill Creek, while ER increased in Oak Creek. Differences in ER patterns are likely due to interactions between several factors. In Oak Creek, ER likely increases post-storm with temporary inputs of DOC, while in South Fork Mill Creek, DOC input could differ, or disturbances could reach deeper into the stream bed, disturbing heterotrophs. As a result, variations of the P/R ratio were driven by rates of ER. Both streams became more heterotrophic post-storm, with South Fork Mill Creek showing a larger effect from higher flows than Oak Creek. However, the limiting impact of flow and sediment disappeared in both streams over the same time-scale, implying a similar recovery period for P/R ratio, with more rapid recovery rates in South Fork Mill Creek. Overall, our results suggest that underlying lithology affects metabolic processes in small mountain streams and drives variation in heterotrophy through changes in ER.

7 Bibliography

Acuña, V., Giorgi, A., Muñoz, I., Uehlinger, U., & Sabater, S. (2004). Flow extremes and benthic organic matter shape the metabolism of a headwater Mediterranean stream. *Freshwater Biology, 49*(7), 960-971. doi:10.1111/j.1365-2427.2004.01239.x

Appling, A. P., Hall Jr., R. O., Yackulic, C. B., & Arroita, M. (2018). Overcoming Equifinality: Leveraging Long Time Series for Stream Metabolism Estimation. *Journal of Geophysical Research: Biogeosciences, 123*(2), 624-645. doi:10.1002/2017jg004140

Atkinson, B. L., Grace, M. R., Hart, B. T., & Vanderkruk, K. E. N. (2008). Sediment instability affects the rate and location of primary production and respiration in a sand-bed stream. *Journal of the North American Benthological Society, 27*(3), 581-592. doi:10.1899/07-143.1

Bair, R. T., Segura, C., & Lorion, C. M. (2019). Quantifying the restoration success of wood introductions to increase coho salmon winter habitat. *Earth Surf. Dynam., 7*(3), 841-857. doi:10.5194/esurf-7-841-2019

Beaulieu, J. J., Arango, C. P., Balz, D. A., & Shuster, W. D. (2013). Continuous monitoring reveals multiple controls on ecosystem metabolism in a suburban stream. *Freshwater Biology, 58*(5), 918-937. doi:10.1111/fwb.12097

Bernhardt, E. S., Heffernan, J. B., Grimm, N. B., Stanley, E. H., Harvey, J. W., Arroita, M., . . . Yackulic, C. B. (2018). The metabolic regimes of flowing waters. *Limnology and Oceanography, 63*(S1), S99-S118. doi:10.1002/lno.10726

Bernot, M. J., Sobota, D. J., Hall Jr, R. O., Mulholland, P. J., Dodds, W. K., Webster, J. R., . . . Wilson, K. (2010). Inter-regional comparison of land-use effects on stream metabolism. *Freshwater Biology, 55*(9), 1874-1890. doi:10.1111/j.1365-2427.2010.02422.x

Biggs, B. J. F. (1995). The contribution of flood disturbance, catchment geology and land use to the habitat template of periphyton in stream ecosystems. *Freshwater Biology, 33*(3), 419-438. doi:10.1111/j.1365-2427.1995.tb00404.x

Biggs, B. J. F., & Close, M. E. (1989). Periphyton biomass dynamics in gravel bed rivers: the relative effects of flows and nutrients. *Freshwater Biology, 22*(2), 209-231. doi:10.1111/j.1365-2427.1989.tb01096.x

Biggs, B. J. F., Smith, R. A., & Duncan, M. J. (1999). Velocity and Sediment Disturbance of Periphyton in Headwater Streams: Biomass and Metabolism. *Journal of the North American Benthological Society, 18*(2), 222-241. doi:10.2307/1468462

Biggs, B. J. F., & Thomsen, H. A. (1995). DISTURBANCE OF STREAM PERIPHYTON BY PERTURBATIONS IN SHEAR STRESS: TIME TO STRUCTURAL FAILURE AND DIFFERENCES IN COMMUNITY RESISTANCE. *Journal of Phycology, 31*(2), 233-241. doi:10.1111/j.0022-3646.1995.00233.x

Blaszczak, J. R., Delesantro, J. M., Urban, D. L., Doyle, M. W., & Bernhardt, E. S. (2019). Scoured or suffocated: Urban stream ecosystems oscillate between hydrologic and dissolved oxygen extremes. *Limnology and Oceanography, 64*(3), 877-894. doi:10.1002/lno.11081

Cade, B. S., & Noon, B. R. (2003). A gentle introduction to quantile regression for ecologists. *Frontiers in Ecology and the Environment, 1*(8), 412-420. doi:10.1890/1540-9295(2003)001[0412:Agitqr]2.0.Co;2

Cade, B. S., Terrell, J. W., & Schroeder, R. L. (1999). ESTIMATING EFFECTS OF LIMITING FACTORS WITH REGRESSION QUANTILES. *Ecology, 80*(1), 311-323. doi:10.1890/0012-9658(1999)080[0311:Eeolfw]2.0.Co;2

Clausen, B., & Biggs, B. J. F. (1997). Relationships between benthic biota and hydrological indices in New Zealand streams. *Freshwater Biology, 38*(2), 327-342. doi:10.1046/j.1365-2427.1997.00230.x

Curran, J. C., & Wilcock, P. R. (2005). Effect of Sand Supply on Transport Rates in a Gravel-Bed Channel. *Journal of Hydraulic Engineering, 131*(11), 961-967. doi:doi:10.1061/(ASCE)0733-9429(2005)131:11(961)

Dingman, S. L. (2002). Physical Hydrology . Long Grove, IL. In: Waveland Press, Inc.

Francoeur, S. N., & Biggs, B. J. F. (2006). Short-term Effects of Elevated Velocity and Sediment Abrasion on Benthic Algal Communities. *Hydrobiologia, 561*(1), 59-69. doi:10.1007/s10750-005-1604-4

Glasmann, J. R., & Simonson, G. H. (1985). Alteration of Basalt in Soils of Western Oregon. *Soil Science Society of America Journal, 49*(1), 262-273. doi:10.2136/sssaj1985.03615995004900010053x

Grace, M. R., Giling, D. P., Hladyz, S., Caron, V., Thompson, R. M., & Mac Nally, R. (2015). Fast processing of diel oxygen curves: Estimating stream metabolism with BASE (BAyesian Single-station Estimation). *Limnology and Oceanography: Methods, 13*(3), e10011. doi:10.1002/lom3.10011

Grimm, N. B., & Fisher, S. G. (1989). Stability of Periphyton and Macroinvertebrates to Disturbance by Flash Floods in a Desert Stream. *Journal of the North American Benthological Society, 8*(4), 293-307. doi:10.2307/1467493

Hall Jr., R. O., Yackulic, C. B., Kennedy, T. A., Yard, M. D., Rosi-Marshall, E. J., Voichick, N., & Behn, K. E. (2015). Turbidity, light, temperature, and hydropeaking control primary productivity in the Colorado River, Grand Canyon. *Limnology and Oceanography, 60*(2), 512-526. doi:10.1002/lno.10031

Hill, B. H., Hall, R. K., Husby, P., Herlihy, A. T., & Dunne, M. (2000). Interregional comparisons of sediment microbial respiration in streams. *Freshwater Biology, 44*(2), 213-222. doi:10.1046/j.1365-2427.2000.00555.x

Holtgrieve, G. W., Schindler, D. E., Branch, T. A., & A'mar, Z. T. (2010). Simultaneous quantification of aquatic ecosystem metabolism and reaeration using a Bayesian statistical model of oxygen dynamics. *Limnology and Oceanography, 55*(3), 1047-1063. doi:10.4319/lo.2010.55.3.1047

Izagirre, O., Agirre, U., Bermejo, M., Pozo, J., & Elosegi, A. (2008). Environmental controls of whole-stream metabolism identified from continuous monitoring of Basque streams. *Journal of the North American Benthological Society, 27*(2), 252-268. doi:10.1899/07-022.1

Katz, S. B., Segura, C., & Warren, D. R. (2018). The influence of channel bed disturbance on benthic Chlorophyll a: A high resolution perspective. *Geomorphology, 305*, 141-153. doi:https://doi.org/10.1016/j.geomorph.2017.11.010

Larned, S. T. (2010). A prospectus for periphyton: recent and future ecological research. *Journal of the North American Benthological Society, 29*(1), 182-206. doi:10.1899/08-063.1

Lisle, T. E., Nelson, J. M., Pitlick, J., Madej, M. A., & Barkett, B. L. (2000). Variability of bed mobility in natural, gravel-bed channels and adjustments to sediment load at

local and reach scales. *Water Resources Research, 36*(12), 3743-3755. doi:10.1029/2000wr900238

Luce, J. J., Cattaneo, A., & Lapointe, M. F. (2010). Spatial patterns in periphyton biomass after low-magnitude flow spates: geomorphic factors affecting patchiness across gravel–cobble riffles. *Journal of the North American Benthological Society, 29*(2), 614-626. doi:10.1899/09-059.1

Luce, J. J., Lapointe, M. F., Roy, A. G., & Ketterling, D. B. (2013). The effects of sand abrasion of a predominantly stable stream bed on periphyton biomass losses. *Ecohydrology, 6*(4), 689-699. doi:10.1002/eco.1332

Mcbride, E. F., & Picard, M. D. (1987). Downstream changes in sand composition, roundness, and gravel size in a short-headed, high-gradient stream, northwestern Italy. *Journal of Sedimentary Research, 57*(6), 1018-1026. doi:10.1306/212f8cd3-2b24-11d7-8648000102c1865d

Mcdowell, W. H. (2015). NEON and STREON: opportunities and challenges for the aquatic sciences. *Freshwater Science, 34*(1), 386-391. doi:10.1086/679489

Milhous, R. T. (1973). *Sediment Transport in a Gravel-Bottomed Stream.* (PhD). Oregon State University, Oregon.

Mueller, E. R., & Pitlick, J. (2013). Sediment supply and channel morphology in mountain river systems: 1. Relative importance of lithology, topography, and climate. *Journal of Geophysical Research: Earth Surface, 118*(4), 2325-2342. doi:10.1002/2013jf002843

Mueller, E. R., Smith, M. E., & Pitlick, J. (2016). Lithology-controlled evolution of stream bed sediment and basin-scale sediment yields in adjacent mountain watersheds, Idaho, USA. *Earth Surface Processes and Landforms, 41*(13), 1869-1883. doi:10.1002/esp.3955

Naegeli, M. W., & Uehlinger, U. (1997). Contribution of the Hyporheic Zone to Ecosystem Metabolism in a Prealpine Gravel-Bed-River. *Journal of the North American Benthological Society, 16*(4), 794-804. doi:10.2307/1468172

O'connor, B. L., Harvey, J. W., & Mcphillips, L. E. (2012). Thresholds of flow-induced bed disturbances and their effects on stream metabolism in an agricultural river. *Water Resources Research, 48*(8). doi:10.1029/2011wr011488

O'connor, J. E., Mangano, J. F., Anderson, S. W., Wallick, J. R., Jones, K. L., & Keith, M. K. (2014). Geologic and physiographic controls on bed-material yield, transport, and channel morphology for alluvial and bedrock rivers, western Oregon. *GSA Bulletin, 126*(3-4), 377-397. doi:10.1130/b30831.1

Odum, H. T. (1956). Primary Production in Flowing Waters. *Limnology and Oceanography, 1*(2), 102-117. doi:10.4319/lo.1956.1.2.0102

Parker, G., & Klingeman, P. C. (1982). On why gravel bed streams are paved. *Water Resources Research, 18*(5), 1409-1423. doi:10.1029/WR018i005p01409

Peterson, C. G., & Stevenson, R. J. (1992). Resistance and Resilience of Lotic Algal Communities: Importance of Disturbance Timing and Current. *Ecology, 73*(4), 1445-1461. doi:10.2307/1940689

Power, M. E., & Dietrich, W. E. (2002). Food webs in river networks. *Ecological Research, 17*(4), 451-471. doi:10.1046/j.1440-1703.2002.00503.x

Prism. *Oregon State University*.

Qasem, K., Vitousek, S., O'connor, B., & Hoellein, T. (2019). The effect of floods on ecosystem metabolism in suburban streams. *Freshwater Science, 38*(2), 412-424. doi:10.1086/703459

Raymond, P. A., & Saiers, J. E. (2010). Event controlled DOC export from forested watersheds. *Biogeochemistry, 100*(1), 197-209. doi:10.1007/s10533-010-9416-7

Raymond, P. A., Zappa, C. J., Butman, D., Bott, T. L., Potter, J., Mulholland, P., . . . Newbold, D. (2012). Scaling the gas transfer velocity and hydraulic geometry in streams and small rivers. *Limnology and Oceanography: Fluids and Environments, 2*(1), 41-53. doi:10.1215/21573689-1597669

Roberts, B. J., Mulholland, P. J., & Hill, W. R. (2007). Multiple Scales of Temporal Variability in Ecosystem Metabolism Rates: Results from 2 Years of Continuous Monitoring in a Forested Headwater Stream. *Ecosystems, 10*(4), 588-606. doi:10.1007/s10021-007-9059-2

Segura, C., Mccutchan, J. H., Lewis Jr, W. M., & Pitlick, J. (2011). The influence of channel bed disturbance on algal biomass in a Colorado mountain stream. *Ecohydrology, 4*(3), 411-421. doi:10.1002/eco.142

Segura, C., & Pitlick, J. (2015). Coupling fluvial-hydraulic models to predict gravel transport in spatially variable flows. *Journal of Geophysical Research: Earth Surface, 120*(5), 834-855. doi:10.1002/2014jf003302

Snavely, P. D., Wagner, H. C., & Macleod, N. S. (1964). Rhythmic-bedded eugeosynclinal deposits of the Tyee formation, Oregon Coast Range. *Kansas Geological Survey Bulletin, 169*, 461-480.

Tett, P., Gallegos, C., Kelly, M. G., Hornberger, G. M., & Cosby, B. J. (1978). Relationships among substrate, flow, and benthic microalgal pigment density in the Mechums River, Virginia. *Limnology and Oceanography, 23*(4), 785-797. doi:10.4319/lo.1978.23.4.0785

Uehlinger, U. (2000). Resistance and resilience of ecosystem metabolism in a flood-prone river system. *Freshwater Biology, 45*(3), 319-332. doi:10.1111/j.1365-2427.2000.00620.x

Uehlinger, U. (2006). Annual cycle and inter-annual variability of gross primary production and ecosystem respiration in a floodprone river during a 15-year period. *Freshwater Biology, 51*(5), 938-950. doi:10.1111/j.1365-2427.2006.01551.x

Uehlinger, U., Kawecka, B., & Robinson, C. T. (2003). Effects of experimental floods on periphyton and stream metabolism below a high dam in the Swiss Alps (River Spöl). *Aquatic Sciences, 65*(3), 199-209. doi:10.1007/s00027-003-0664-7

Uehlinger, U., & Naegeli, M. W. (1998). Ecosystem Metabolism, Disturbance, and Stability in a Prealpine Gravel Bed River. *Journal of the North American Benthological Society, 17*(2), 165-178. doi:10.2307/1467960

Uehlinger, U., Naegeli, M. W., & Fisher, S. G. (2002). A heterotrophic desert stream? The role of sediment stability. *Western North American Naturalist, 62*(4), 466-473.

Vannote, R. L., Minshall, G. W., Cummins, K. W., Sedell, J. R., & Cushing, C. E. (1980). The River Continuum Concept. *Canadian Journal of Fisheries and Aquatic Sciences, 37*(1), 130-137. doi:10.1139/f80-017

Walker, G., & Macleod, N. (Cartographer). (1991). Geologic Map of Oregon: US Geological Survey, scale 1:500,000

Webster, J. R., & Meyer, J. L. (1997). Organic Matter Budgets for Streams: A Synthesis. *Journal of the North American Benthological Society, 16*(1), 141-161. doi:10.2307/1468247

Wilcock, P. R., Kenworthy, S. T., & Crowe, J. C. (2001). Experimental study of the transport of mixed sand and gravel. *Water Resources Research, 37*(12), 3349-3358. doi:10.1029/2001wr000683

8 Appendices

Appendix A – Time Series Data

In Oak Creek, we collected 10-minute interval dissolved oxygen (DO), photosynthetically active radiation (PAR), and water temperature data from December 2017 to May 2018 and from December 2018 to May 2019. In South Fork Mill Creek, we collected the same data from December 2018 to May 2019. During these time periods, we also measured water depth to calculate discharge, and collected water samples to calculate suspended sediment concentration. These data were used to model GPP and ER during the study periods.

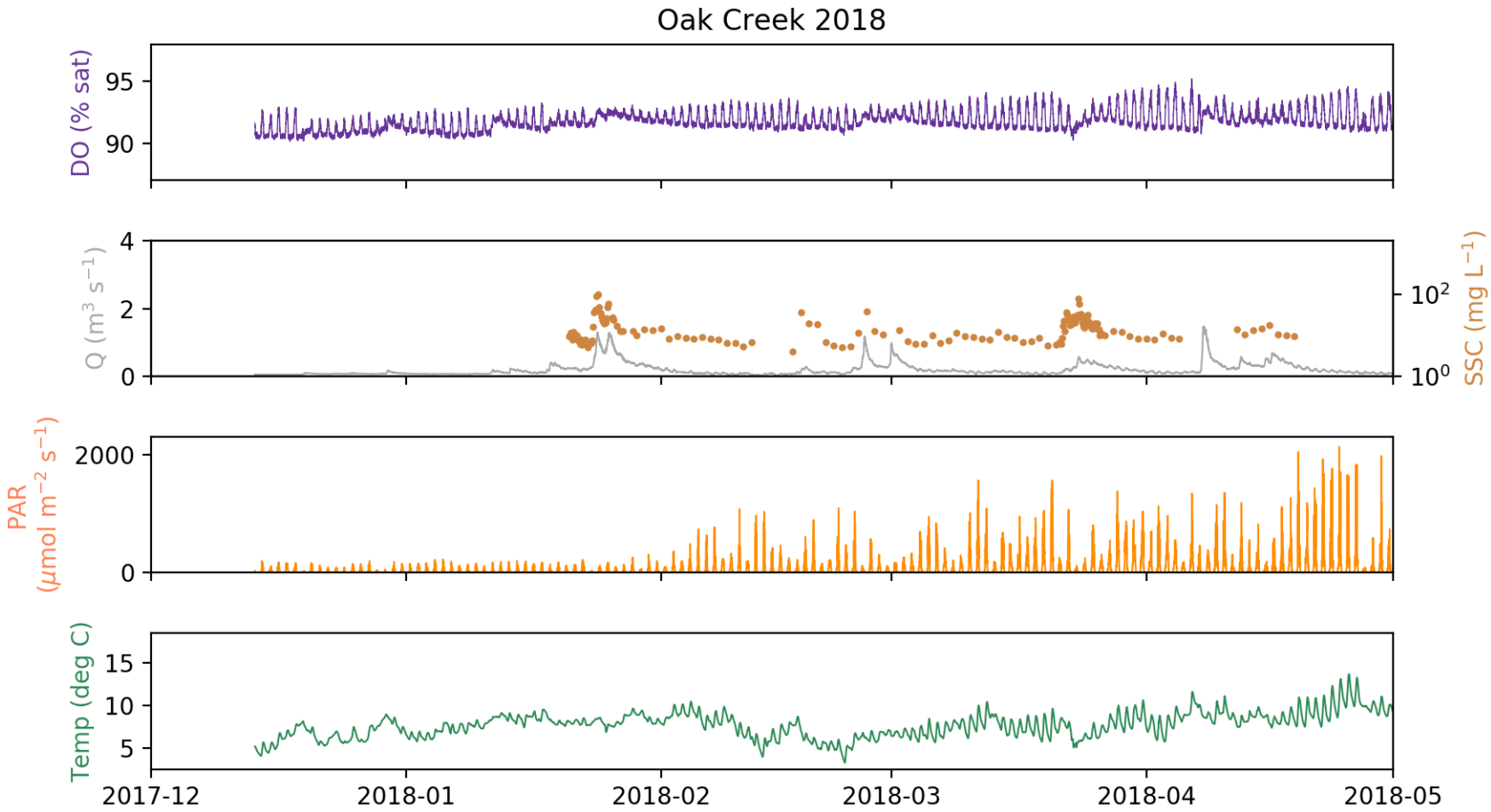

Figure A.1 Physical attribute data collected in Oak Creek between December 2017 and May 2018. DO (% saturated), PAR (µmol m^{-2} s^{-1}), water temperature (degrees Celsius), and depth to calculate discharge (m^3 s^{-1}) were collected at 10-minute intervals. SSC samples (mg L^{-1}) were collected daily at midnight or with higher frequency during storms.

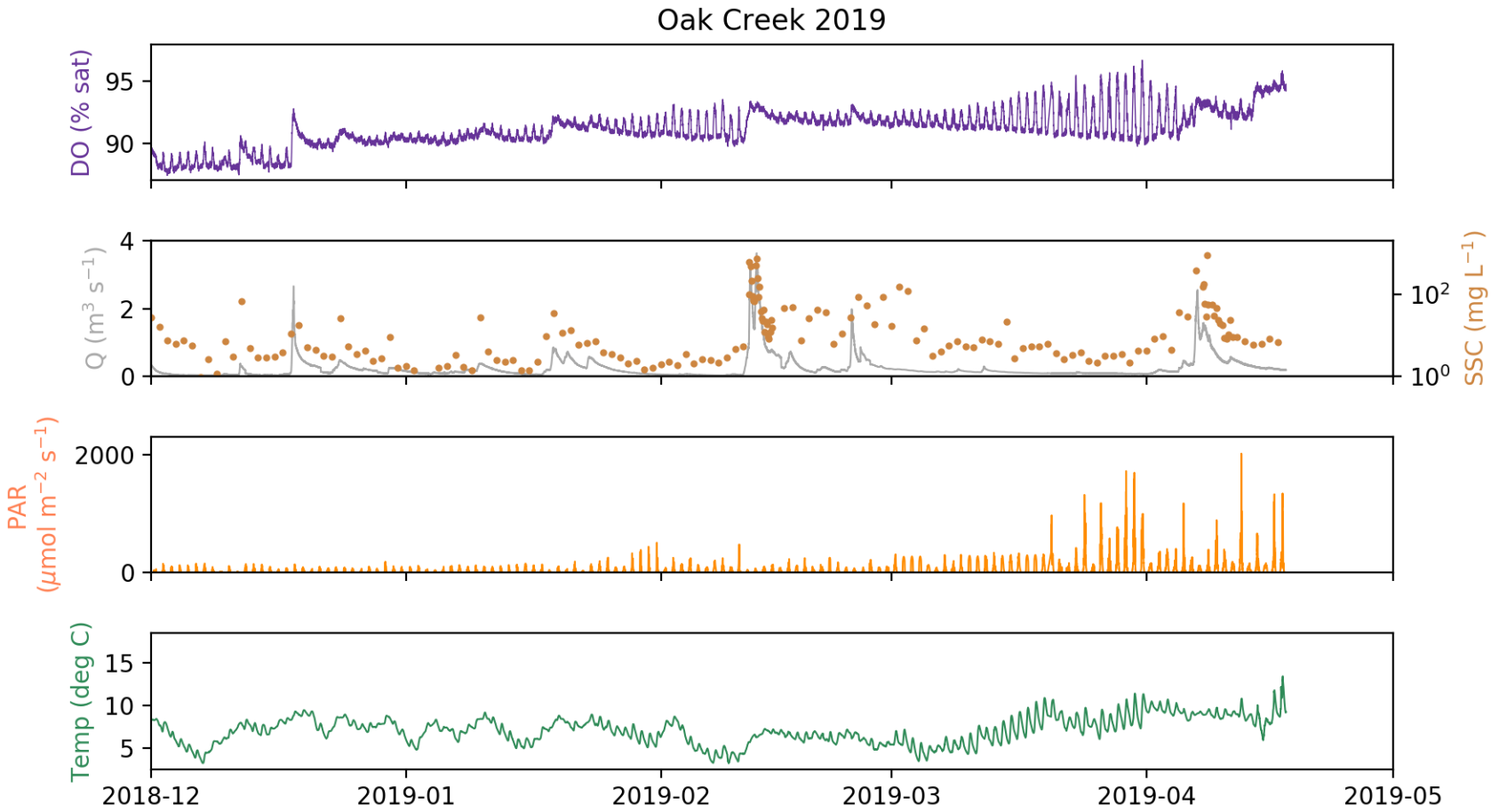

Figure A.2 Physical attribute data collected in Oak Creek between December 2018 and May 2019. DO (% saturated), PAR (µmol m^{-2} s^{-1}), water temperature (degrees Celsius), and depth to calculate discharge (m^3 s^{-1}) were collected at 10-minute intervals. SSC samples (mg L^{-1}) were collected daily at midnight or with higher frequency during storms.

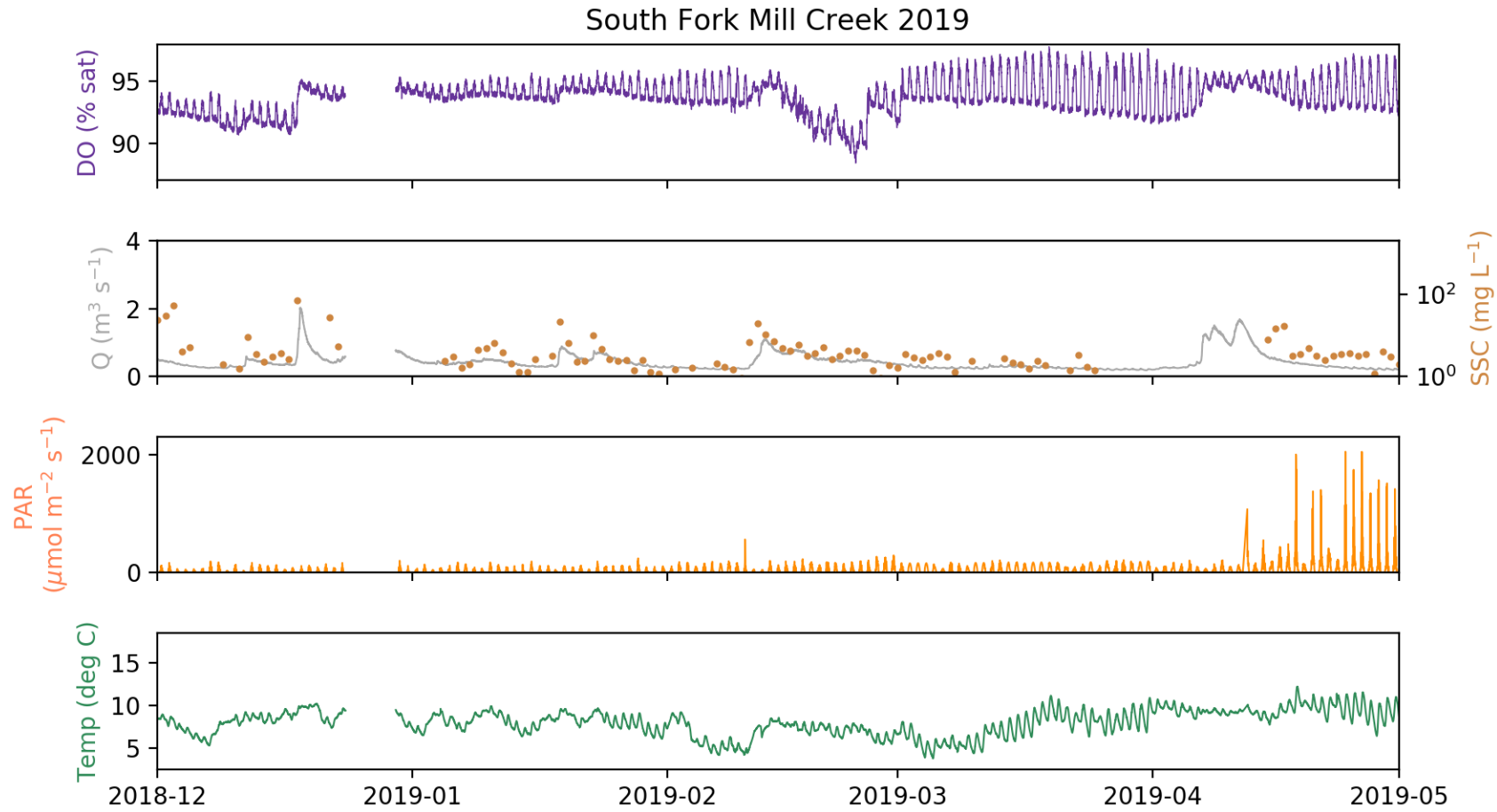

Figure A.3 Physical attribute data collected in South Fork Mill Creek between December 2018 and May 2019. DO (% saturated), PAR (µmol m^{-2} s^{-1}), water temperature (degrees Celsius), and depth to calculate discharge (m^3 s^{-1}) were collected at 10-minute intervals. SSC samples (mg L^{-1}) were collected daily at midnight or with higher frequency during storms.

Appendix B – Data Gap Filling

8.2.1 Gaps in PAR Data

There were gaps in collected PAR data in Oak Creek for 34 days between February and March 2019, and in South fork Mill Creek for 43 days between March and April 2019. Gaps were filled by estimating PAR through a relationship with solar radiation data collected from nearby meteorological stations. The station used for Oak Creek was 0.8 km away, and the other station was 21 km away from South Fork Mill Creek (Table B1). Both relationship were best represented by a power-law relationship (PAR = aSR^b). In Oak Creek, a=0.88 and b=0.88 with r^2=0.85 (Figure B1a). In South Fork Mill Creek, a=1.47, and b=0.73 with r^2=0.70 (Figure B1b).

Table B.1 Locations of meteorological stations used to create relationships with PAR.

For Oak Creek	44° 36’ 44.5098”, -123° 19’ 55.5348”
For South Fork Mill Creek	44° 35’ 39.9726”, -123° 36’ 47.8974”

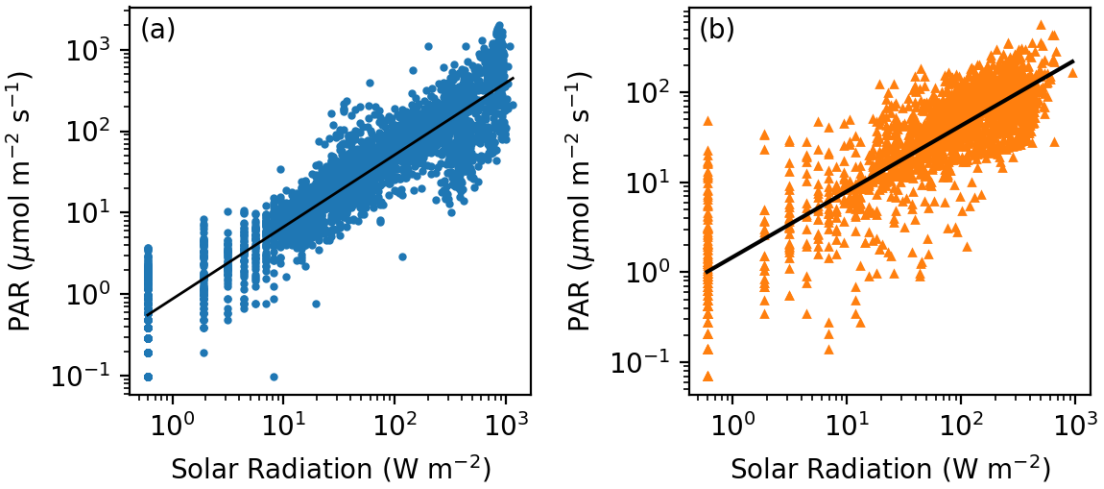

Figure B.1 Relationships built between solar radiation (W m^{-2}) at nearby meteorological stations and PAR (µmol m^{-2} s^{-1}) reaching the stream, fit with a power-law relationship (PAR = aSR^b). For Oak Creek (a), the best-fit line (a=0.88, b=0.88, r^2=0.85) was used to calculate PAR data during a gap of 34 days from February to March 2019. For South Fork Mill Creek (b), the best-fit line (a=1.47, b=0.73, r^2=0.70) was used to calculate PAR data during a gap of 43 days between March and April 2019.

8.2.2 Gap in Oak Creek Discharge Data

There was a gap in the depth data collected for Oak Creek during a period from February to March 2019. This gap was filled by creating a relationship with the depth at a downstream pressure transducer 5 km away (44° 33’ 59.5326”, -123° 18’ 2.97”) and using the relationship to calculate depth in our reach. The best fit was a power-law relationship with the coefficients a=0.24 and b=2.33 with r^2=0.88 (Figure B2).

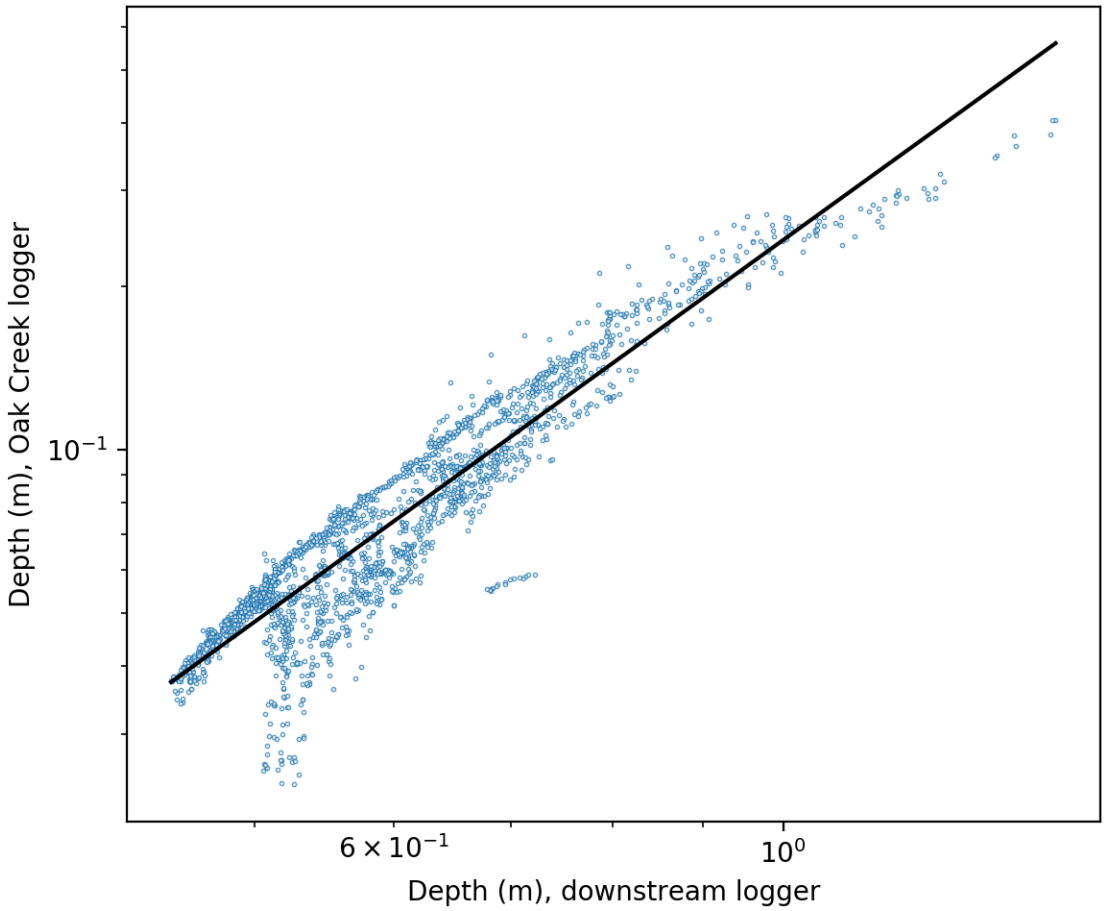

Figure B.2 Relationship between Oak Creek pressure transducer and downstream pressure transducer. The power-law best-fit line (a=0.24, b=2.33, r^2=0.88) was used to calculate depth in Oak Creek during a gap in data from February to March 2019.

Appendix C – Sulfur Hexafluoride Releases

8.3.1 Data Collection

Sulfur hexafluoride gas release data were collected and analyzed according to the procedure outlined in Section 3.2.2. Three gas releases were completed in Oak Creek (2015 – Heaston, 2018 & 2019 – Cargill), and one gas release was completed in South Fork Mill Creek (2019 – Cargill).

8.3.2 Data Summary

Gas release and gas chromatograph analyses are located in the Segura_Lab folder in the T: drive, in an Excel workbook and in two .csv files, in the location T:\Groups\Segura_Lab\2017_Sediment_Transport_Ecology\SF6_Release_Data.

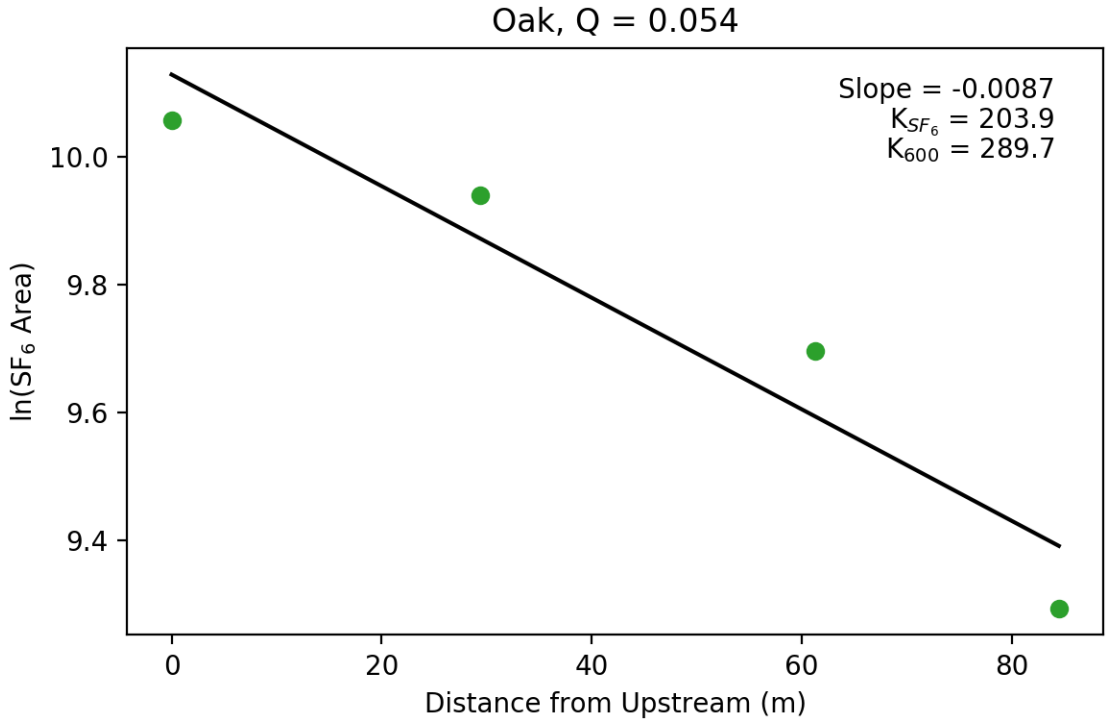

Figure C.1 K_{600} value of 289.7 from SF_6 release in Oak Creek on July 10, 2015 at a discharge of 0.054 m^3/s.

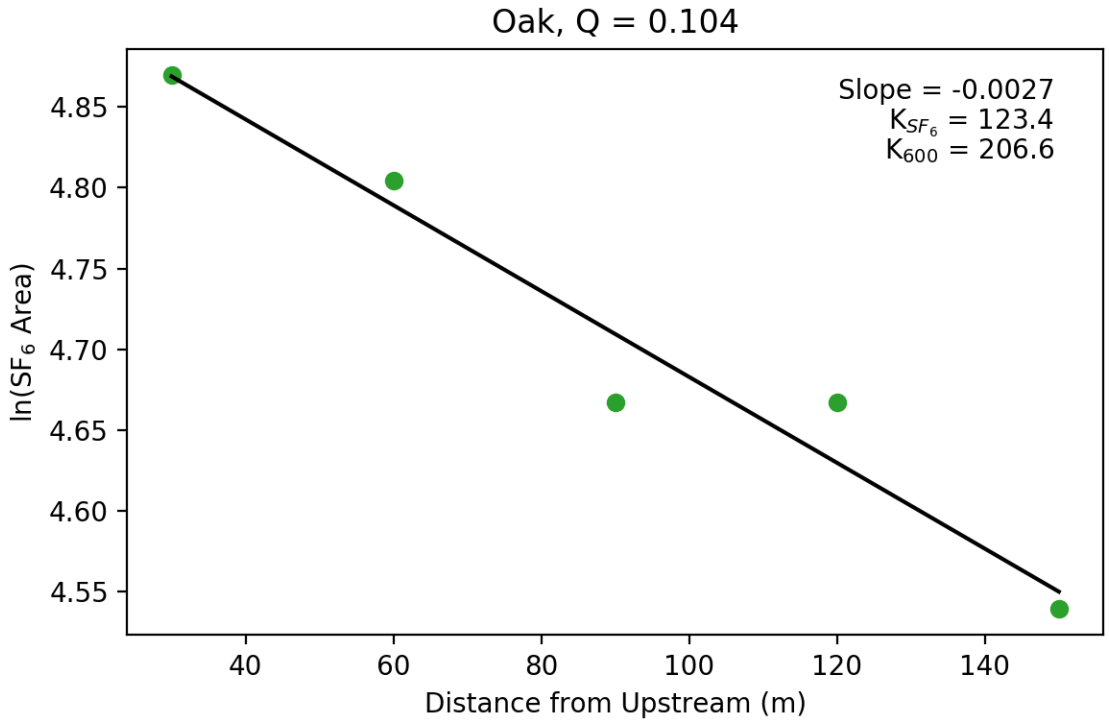

Figure C.2 K_{600} value of 206.6 from SF_6 release in Oak Creek on May 1, 2018 at a discharge of 0.104 m^3/s.

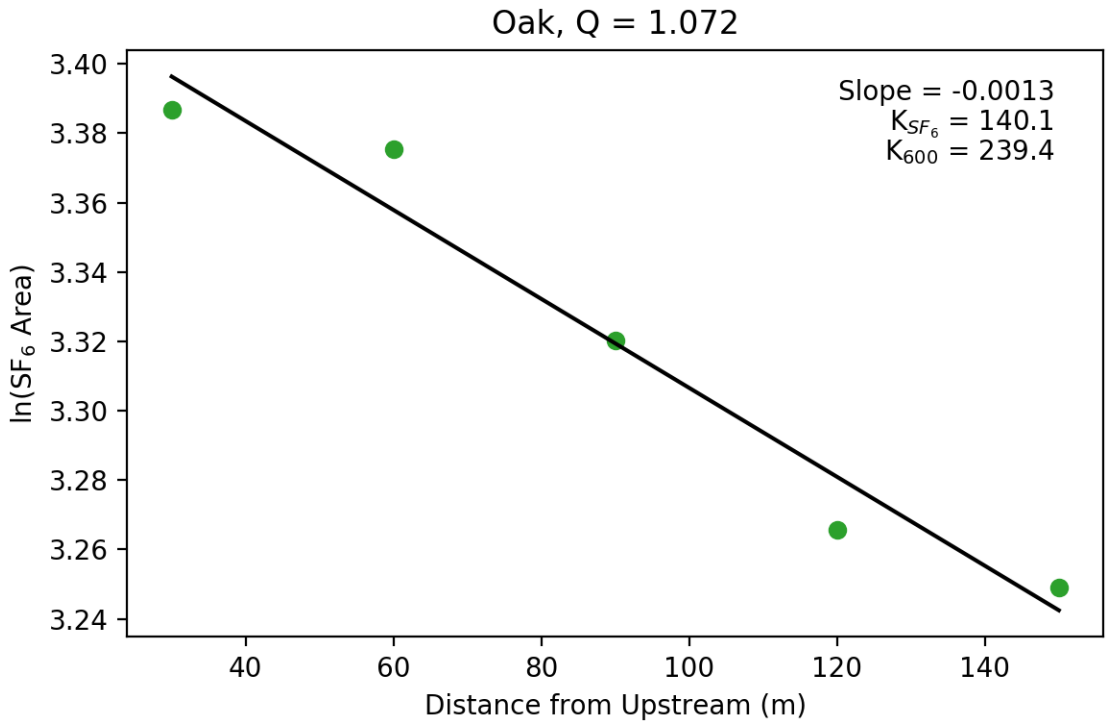

Figure C.3 K_{600} value of 239.4 from SF_6 release in Oak Creek on April 8, 2019 at a discharge of 1.072 m^3/s.

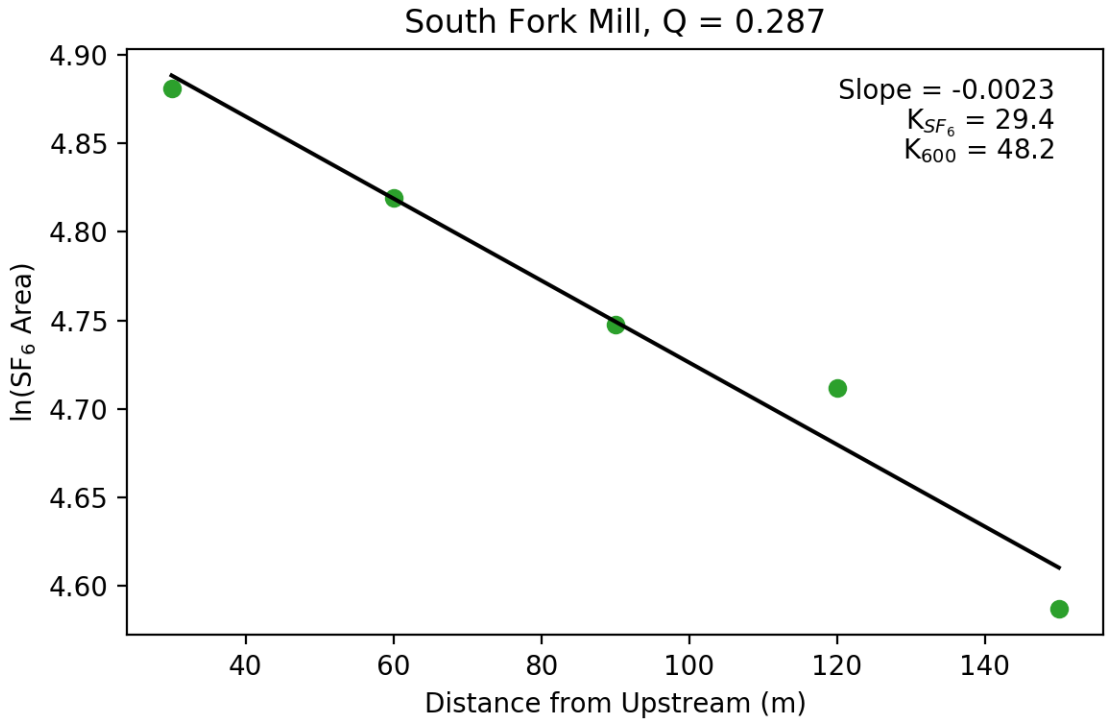

Figure C.4 K_{600} value of 48.2 from SF_6 release in South Fork Mill Creek on April 23, 2019 at a discharge of 0.287 m^3/s.

Appendix D – Quantile Regression Selection

The 80th quantile in our analysis was chosen as the upper-most quantile before sampling variation began to increase, as stated in Section 3.3.1. The following are examples of the confidence bounds calculated and plotted for each quantile to show the variation increases in higher quantiles.

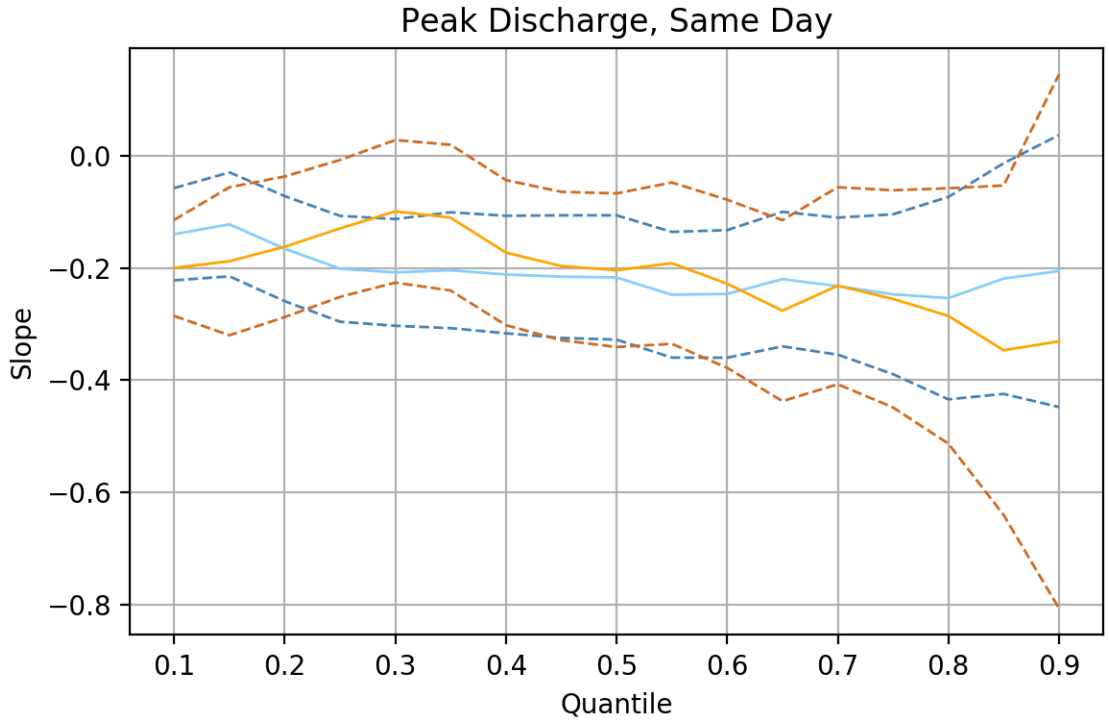

Figure D.1 95% confidence bounds for quantile regressions between the 0.1 and 0.9 quantiles between GPP and maximum same-day discharge. Blue represents Oak Creek, while orange represents South Fork Mill Creek. Solid lines represent the slope of the calculated quantile, while the dashed lines are the 95% confidence bounds.

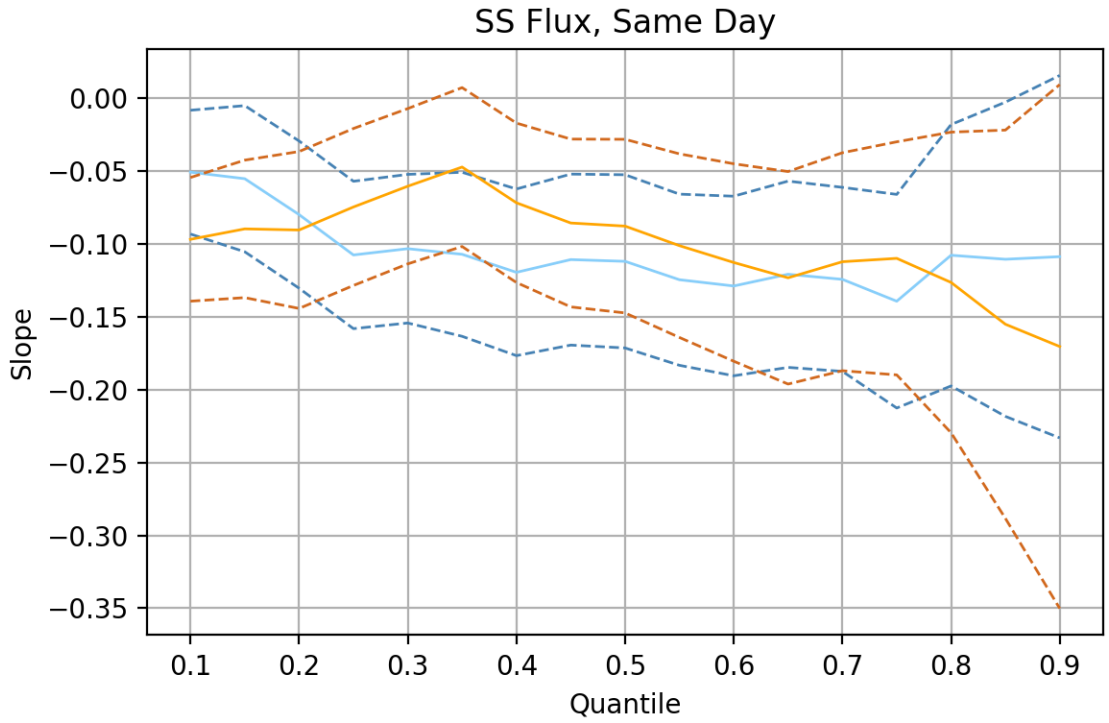

Figure D.2 95% confidence bounds for quantile regressions between the 0.1 and 0.9 quantiles between GPP and same-day suspended sediment flux. Blue represents Oak Creek, while orange represents South Fork Mill Creek. Solid lines represent the slope of the calculated quantile, while the dashed lines are the 95% confidence bounds.

Appendix E – Model Results

Table E.1 Modeling results from Oak Creek in 2018. RMSEs were calculated from observed and modeled dissolved oxygen curves in mg L^{-1}. $\hat{R}$ values should be less than 1.1 and close to 1.0 for good model fits.

Date	GPP (g O_2 m^{-2} d^{-1})	ER (g O_2 m^{-2} d^{-1})	K_{600} (day^{-1})	RMSE (mg L^{-1} O_2)	GPP $\hat{R}$	ER $\hat{R}$	K_{600} $\hat{R}$
12/14/2017	0.34	-8.75	267.69	0.025	1.0034	1.0034	1.0034
12/15/2017	0.35	-9.97	306.58	0.018	1.0009	1.0009	1.0009
12/16/2017	0.42	-9.05	278.54	0.023	1.0009	1.0009	1.0009
12/17/2017	0.48	-9.55	293.92	0.021	1.0001	0.9999	1.0000
12/18/2017	0.43	-8.66	265.80	0.025	1.0008	1.0006	1.0005
12/20/2017	0.14	-9.45	226.38	0.027	1.0000	1.0005	1.0005
12/21/2017	0.20	-9.30	241.25	0.026	0.9999	1.0002	1.0002
12/22/2017	0.23	-7.27	190.46	0.040	1.0002	1.0010	1.0010
12/23/2017	0.18	-11.15	271.25	0.021	1.0024	1.0029	1.0029
12/24/2017	0.23	-9.43	233.34	0.028	1.0009	1.0009	1.0010
12/25/2017	0.22	-12.57	301.55	0.016	1.0014	1.0006	1.0005
12/26/2017	0.20	-9.63	245.73	0.024	1.0002	1.0006	1.0006
12/27/2017	0.31	-10.38	269.03	0.020	1.0002	1.0002	1.0002
12/28/2017	0.23	-8.88	227.97	0.028	1.0018	1.0015	1.0014
12/30/2017	0.03	-6.96	152.80	0.041	0.9998	1.0006	1.0006
12/31/2017	0.20	-10.35	250.77	0.022	1.0004	1.0002	1.0002
1/1/2018	0.19	-10.52	267.48	0.020	1.0003	1.0000	1.0000
1/2/2018	0.44	-11.80	310.49	0.015	1.0006	0.9999	0.9999
1/3/2018	0.30	-10.17	276.26	0.020	0.9997	0.9997	0.9997
1/4/2018	0.35	-9.98	278.62	0.021	1.0000	1.0002	1.0002
1/5/2018	0.22	-8.92	229.95	0.028	1.0013	1.0011	1.0010
1/6/2018	0.28	-9.31	244.66	0.025	0.9999	1.0000	1.0000
1/7/2018	0.43	-11.01	297.19	0.017	1.0003	1.0009	1.0009
1/8/2018	0.37	-9.06	250.22	0.024	1.0004	1.0003	1.0003
1/9/2018	0.25	-9.99	249.75	0.023	1.0022	1.0021	1.0020
1/10/2018	0.33	-12.15	315.61	0.015	1.0004	1.0008	1.0008
1/12/2018	0.04	-6.28	131.87	0.046	0.9998	1.0003	1.0003
1/14/2018	0.06	-6.58	112.05	0.049	1.0008	1.0006	1.0005
1/15/2018	0.07	-7.81	154.58	0.037	0.9995	0.9996	0.9996
1/16/2018	0.21	-6.81	153.52	0.046	0.9998	1.0003	1.0003
1/28/2018	0.02	-7.37	82.98	0.047	0.9995	1.0002	1.0002
2/3/2018	0.18	-8.39	176.93	0.032	0.9996	1.0000	1.0001
2/5/2018	0.08	-6.46	164.65	0.043	0.9997	0.9998	0.9998

Date	GPP (g O_2 m^{-2} d^{-1})	ER (g O_2 m^{-2} d^{-1})	K_{600} (day^{-1})	RMSE (mg L^{-1} O_2)	GPP $\hat{R}$	ER $\hat{R}$	K_{600} $\hat{R}$
2/24/2018	0.01	-7.76	113.09	0.048	0.9995	1.0009	1.0010
2/27/2018	0.23	-12.59	161.55	0.024	1.0010	1.0014	1.0014
3/7/2018	0.36	-10.01	183.73	0.026	1.0005	1.0018	1.0019
3/13/2018	0.05	-7.80	148.72	0.039	1.0000	1.0006	1.0006
3/14/2018	0.02	-7.50	150.15	0.038	0.9998	1.0001	1.0002
3/24/2018	0.29	-9.39	91.25	0.038	1.0009	1.0014	1.0014
3/25/2018	0.13	-9.29	101.68	0.035	1.0002	1.0013	1.0013
3/26/2018	0.08	-8.56	107.03	0.039	1.0004	1.0011	1.0010
3/27/2018	0.16	-8.23	111.23	0.040	0.9997	0.9997	0.9997
3/28/2018	0.08	-6.83	104.31	0.045	1.0004	1.0004	1.0004
3/29/2018	0.15	-6.41	105.38	0.049	0.9995	0.9996	0.9996
3/30/2018	0.28	-6.45	111.75	0.047	1.0008	1.0012	1.0012
4/9/2018	0.09	-7.97	87.03	0.039	1.0002	1.0004	1.0004
4/11/2018	0.21	-9.31	133.66	0.033	0.9998	1.0003	1.0004
4/13/2018	0.06	-9.58	108.88	0.035	0.9997	0.9997	0.9997
4/14/2018	0.29	-12.02	147.55	0.026	1.0010	1.0016	1.0015
4/16/2018	0.02	-8.79	73.60	0.040	0.9995	0.9998	0.9997
4/17/2018	0.05	-10.88	107.38	0.031	0.9996	0.9997	0.9997
4/20/2018	0.02	-6.65	104.76	0.046	0.9998	0.9998	0.9998
4/21/2018	0.00	-6.38	113.57	0.046	0.9997	1.0007	1.0006

Table E.2 Modeling results from Oak Creek in 2019. RMSEs were calculated from observed and modeled dissolved oxygen curves in mg L^{-1}. $\hat{R}$ values should be less than 1.1 and close to 1.0 for good model fits.

Date	GPP (g O_2 m^{-2} d^{-1})	ER (g O_2 m^{-2} d^{-1})	K_{600} (day^{-1})	RMSE (mg L^{-1} O_2)	GPP $\hat{R}$	ER $\hat{R}$	K_{600} $\hat{R}$
12/6/2018	0.10	-8.60	268.08	0.032	1.0008	1.0020	1.0020
12/7/2018	0.24	-9.58	316.52	0.023	1.0014	1.0016	1.0015
12/8/2018	0.17	-10.15	330.45	0.021	1.0002	1.0009	1.0009
12/20/2018	0.02	-12.38	120.64	0.033	0.9994	0.9999	0.9999
1/3/2019	0.02	-7.80	182.93	0.038	0.9996	1.0003	1.0003
1/5/2019	0.05	-6.59	141.11	0.048	0.9996	1.0004	1.0005
1/7/2019	0.09	-8.88	158.33	0.033	0.9997	1.0000	1.0000
1/8/2019	0.02	-12.10	180.95	0.024	0.9995	1.0003	1.0003
1/13/2019	0.01	-6.97	138.32	0.050	0.9997	0.9999	0.9998
1/16/2019	0.21	-9.02	263.87	0.025	0.9997	0.9997	0.9997

Date	GPP (g O_2 m^{-2} d^{-1})	ER (g O_2 m^{-2} d^{-1})	K_{600} (day^{-1})	RMSE (mg L^{-1} O_2)	GPP $\hat{R}$	ER $\hat{R}$	K_{600} $\hat{R}$
1/24/2019	0.05	-7.52	82.54	0.049	0.9999	1.0002	1.0002
1/26/2019	0.08	-7.44	117.97	0.047	0.9999	1.0014	1.0013
1/27/2019	0.11	-7.80	144.39	0.042	0.9997	1.0009	1.0010
1/28/2019	0.18	-7.76	164.39	0.037	0.9999	1.0001	1.0001
1/29/2019	0.08	-6.55	158.99	0.045	1.0009	1.0006	1.0005
1/30/2019	0.08	-6.33	174.88	0.043	0.9999	0.9998	0.9998
1/31/2019	0.10	-5.70	177.07	0.047	1.0011	1.0028	1.0026
2/1/2019	0.32	-8.85	288.88	0.022	1.0025	1.0027	1.0027
2/2/2019	0.26	-5.61	199.12	0.044	1.0005	1.0009	1.0008
2/4/2019	0.24	-5.99	180.24	0.047	1.0002	1.0000	1.0000
2/5/2019	0.29	-6.39	216.18	0.042	1.0007	1.0005	1.0004
2/6/2019	0.24	-5.51	216.55	0.049	1.0010	1.0015	1.0014
2/7/2019	0.36	-5.99	262.83	0.037	1.0039	1.0045	1.0043
2/27/2019	0.13	-9.26	119.21	0.037	0.9997	1.0001	1.0001
3/1/2019	0.20	-11.85	182.64	0.024	1.0005	1.0008	1.0009
3/2/2019	0.14	-12.29	201.04	0.022	1.0006	1.0019	1.0019
3/3/2019	0.13	-11.19	197.13	0.025	1.0002	1.0011	1.0011
3/4/2019	0.16	-11.88	226.16	0.021	1.0002	1.0008	1.0008
3/5/2019	0.30	-11.90	240.87	0.019	1.0017	1.0017	1.0016
3/6/2019	0.14	-9.15	184.24	0.031	1.0002	1.0008	1.0007
3/7/2019	0.20	-8.63	171.80	0.033	1.0001	1.0000	1.0000
3/10/2019	0.23	-10.47	203.74	0.025	1.0005	1.0010	1.0010
3/13/2019	0.25	-8.72	158.60	0.031	1.0007	1.0017	1.0018
3/14/2019	0.36	-8.54	167.34	0.033	0.9999	1.0001	1.0001
3/15/2019	0.49	-9.63	200.98	0.027	0.9998	1.0003	1.0003
3/16/2019	0.42	-6.91	151.32	0.042	1.0003	1.0003	1.0002
3/17/2019	0.54	-8.99	202.46	0.028	1.0007	1.0006	1.0006
3/18/2019	0.58	-8.57	201.00	0.028	0.9998	0.9998	0.9998
3/21/2019	0.58	-6.74	158.96	0.042	1.0013	1.0016	1.0015
3/22/2019	0.60	-6.40	145.25	0.047	1.0008	1.0013	1.0012
3/25/2019	0.82	-9.15	210.15	0.027	1.0013	1.0012	1.0012
4/2/2019	0.40	-7.59	123.44	0.044	0.9999	0.9998	0.9998
4/3/2019	0.69	-7.06	123.69	0.045	1.0011	1.0010	1.0011
4/10/2019	0.32	-9.82	101.33	0.033	1.0007	1.0014	1.0014
4/12/2019	0.07	-9.35	106.33	0.031	1.0000	1.0011	1.0011
4/15/2019	0.21	-9.88	199.05	0.024	1.0001	1.0003	1.0003
4/16/2019	0.03	-6.97	155.36	0.036	0.9997	1.0005	1.0006

Table E.3 Modeling results from South Fork Mill Creek 2019. RMSEs were calculated from observed and modeled dissolved oxygen curves in mg L^{-1}. $\hat{R}$ values should be less than 1.1 and close to 1.0 for good model fits.

Date	GPP (g O_2 m^{-2} d^{-1})	ER (g O_2 m^{-2} d^{-1})	K_{600} (day^{-1})	RMSE (mg L^{-1} O_2)	GPP $\hat{R}$	ER $\hat{R}$	K_{600} $\hat{R}$
12/1/2018	0.19	-7.18	33.39	0.022	0.9998	0.9996	0.9996
12/2/2018	0.18	-7.32	34.79	0.033	1.0002	1.0003	1.0003
12/3/2018	0.15	-7.71	37.54	0.022	0.9995	0.9996	0.9996
12/4/2018	0.14	-6.76	33.95	0.024	0.9996	1.0002	1.0003
12/5/2018	0.16	-6.14	31.36	0.029	0.9997	0.9997	0.9997
12/6/2018	0.16	-5.66	29.29	0.033	1.0001	1.0002	1.0002
12/7/2018	0.24	-5.23	26.69	0.043	1.0022	1.0024	1.0022
12/8/2018	0.30	-5.98	28.27	0.036	0.9998	0.9999	0.9999
12/9/2018	0.23	-5.74	25.72	0.036	1.0001	1.0001	1.0000
12/10/2018	0.27	-6.83	30.57	0.031	0.9997	0.9997	0.9997
12/11/2018	0.17	-6.64	28.28	0.039	0.9999	0.9996	0.9997
12/12/2018	0.20	-8.27	34.21	0.022	1.0004	1.0003	1.0003
12/13/2018	0.22	-8.53	35.91	0.026	1.0005	1.0014	1.0014
12/14/2018	0.22	-8.47	36.94	0.022	1.0004	1.0001	1.0001
12/15/2018	0.30	-8.13	34.94	0.022	1.0010	1.0008	1.0007
12/16/2018	0.26	-7.62	32.21	0.026	0.9996	0.9997	0.9997
12/17/2018	0.25	-7.10	30.32	0.036	1.0013	1.0022	1.0021
12/19/2018	0.03	-5.53	26.25	0.017	0.9998	0.9999	0.9999
12/20/2018	0.09	-5.62	30.04	0.027	0.9998	0.9999	0.9998
12/21/2018	0.05	-6.19	34.35	0.017	1.0003	1.0007	1.0007
12/22/2018	0.15	-6.02	32.07	0.026	1.0007	1.0009	1.0009
12/30/2018	0.05	-5.45	29.47	0.022	1.0006	1.0006	1.0005
1/2/2019	0.14	-6.29	35.72	0.025	1.0003	1.0000	1.0000
1/3/2019	0.10	-6.16	34.78	0.019	0.9997	1.0005	1.0005
1/5/2019	0.10	-6.26	37.31	0.029	1.0000	1.0005	1.0005
1/6/2019	0.10	-6.09	36.40	0.027	1.0005	1.0011	1.0012
1/7/2019	0.15	-6.03	35.01	0.026	1.0001	1.0001	1.0002
1/8/2019	0.15	-6.18	34.48	0.021	1.0001	1.0008	1.0007
1/9/2019	0.17	-5.89	32.64	0.019	0.9999	1.0004	1.0004
1/10/2019	0.19	-5.87	32.89	0.019	1.0008	1.0004	1.0004
1/11/2019	0.15	-5.84	33.67	0.023	1.0008	1.0003	1.0004
1/12/2019	0.12	-6.23	37.12	0.021	0.9998	1.0002	1.0001
1/13/2019	0.10	-6.27	37.78	0.026	1.0005	1.0013	1.0012
1/14/2019	0.09	-5.52	34.12	0.025	1.0001	1.0011	1.0011
1/15/2019	0.17	-4.86	31.01	0.033	1.0000	1.0009	1.0009

Date	GPP (g O_2 m^{-2} d^{-1})	ER (g O_2 m^{-2} d^{-1})	K_{600} (day^{-1})	RMSE (mg L^{-1} O_2)	GPP $\hat{R}$	ER $\hat{R}$	K_{600} $\hat{R}$
1/16/2019	0.16	-4.95	30.82	0.026	1.0008	1.0006	1.0004
1/19/2019	0.17	-5.75	29.54	0.020	0.9998	1.0004	1.0003
1/20/2019	0.10	-5.36	30.25	0.023	1.0001	1.0005	1.0004
1/21/2019	0.16	-6.02	34.40	0.027	1.0001	1.0010	1.0011
1/22/2019	0.22	-4.95	26.15	0.032	0.9999	1.0005	1.0006
1/23/2019	0.16	-5.14	27.52	0.031	1.0005	1.0008	1.0008
1/24/2019	0.06	-5.73	32.03	0.018	1.0004	1.0004	1.0004
1/25/2019	0.09	-6.29	35.71	0.026	0.9996	0.9999	0.9999
1/26/2019	0.15	-6.07	35.81	0.023	0.9996	0.9998	0.9998
1/27/2019	0.18	-6.50	38.91	0.027	1.0009	1.0012	1.0011
1/28/2019	0.21	-5.39	33.55	0.025	0.9999	1.0006	1.0006
1/29/2019	0.15	-5.56	34.99	0.031	0.9997	1.0004	1.0005
1/30/2019	0.16	-5.23	33.50	0.035	1.0006	1.0010	1.0010
1/31/2019	0.22	-5.14	32.63	0.039	0.9997	1.0000	1.0001
2/1/2019	0.27	-4.95	30.45	0.021	1.0014	1.0011	1.0011
2/2/2019	0.23	-4.24	27.50	0.035	1.0000	1.0001	1.0001
2/3/2019	0.28	-4.05	27.26	0.037	1.0009	1.0015	1.0016
2/4/2019	0.29	-4.01	26.49	0.029	1.0012	1.0013	1.0013
2/5/2019	0.24	-4.00	27.31	0.040	1.0000	0.9999	1.0000
2/6/2019	0.16	-3.68	25.28	0.041	1.0004	1.0005	1.0005
2/7/2019	0.16	-3.33	22.82	0.046	1.0004	1.0004	1.0005
2/9/2019	0.32	-4.56	29.90	0.030	0.9998	1.0000	1.0001
2/11/2019	0.14	-4.01	21.64	0.042	1.0005	1.0009	1.0008
2/13/2019	0.11	-5.19	26.93	0.020	1.0006	1.0007	1.0006
2/15/2019	0.15	-4.32	19.67	0.047	1.0005	1.0008	1.0007
2/18/2019	0.04	-7.09	25.20	0.046	1.0018	1.0019	1.0018
2/19/2019	0.40	-8.12	28.90	0.026	1.0003	1.0005	1.0005
2/22/2019	0.17	-8.91	30.77	0.035	0.9999	1.0008	1.0008
2/23/2019	0.19	-8.07	26.50	0.048	1.0015	1.0023	1.0023
2/24/2019	0.27	-8.39	28.48	0.028	1.0003	1.0001	1.0001
2/26/2019	0.22	-5.97	31.14	0.032	1.0018	1.0023	1.0021
2/27/2019	0.32	-6.07	30.80	0.041	1.0007	1.0006	1.0005
2/28/2019	0.40	-6.75	31.36	0.033	1.0011	1.0010	1.0009
3/2/2019	0.19	-4.53	30.18	0.038	1.0007	1.0005	1.0005
3/3/2019	0.14	-3.81	26.47	0.049	1.0004	1.0005	1.0006
3/5/2019	0.32	-3.96	27.11	0.037	1.0008	1.0005	1.0004
3/6/2019	0.35	-3.50	24.15	0.044	1.0001	0.9999	0.9998
3/7/2019	0.25	-3.49	24.33	0.048	1.0003	1.0000	1.0000

Date	GPP (g O_2 m^{-2} d^{-1})	ER (g O_2 m^{-2} d^{-1})	K_{600} (day^{-1})	RMSE (mg L^{-1} O_2)	GPP $\hat{R}$	ER $\hat{R}$	K_{600} $\hat{R}$
3/13/2019	0.19	-2.99	20.45	0.049	1.0001	1.0004	1.0004
3/14/2019	0.28	-3.72	24.78	0.047	0.9997	0.9998	0.9998
3/15/2019	0.31	-4.10	27.30	0.048	1.0025	1.0029	1.0029
3/16/2019	0.42	-3.92	25.85	0.045	1.0000	1.0001	1.0000
3/22/2019	0.41	-3.85	23.43	0.039	0.9996	0.9997	0.9997
4/1/2019	0.69	-4.26	22.49	0.049	1.0026	1.0028	1.0027
4/2/2019	0.60	-4.63	24.57	0.037	0.9996	0.9997	0.9998
4/6/2019	0.39	-3.72	18.87	0.049	1.0003	1.0007	1.0008
4/7/2019	0.23	-5.64	26.13	0.027	0.9998	0.9998	0.9997
4/8/2019	0.13	-5.31	24.74	0.021	1.0005	1.0011	1.0011
4/9/2019	0.14	-4.98	23.99	0.020	0.9995	0.9996	0.9996
4/10/2019	0.31	-4.98	22.22	0.027	1.0000	1.0000	1.0000
4/13/2019	0.11	-5.37	28.23	0.022	0.9998	0.9997	0.9997
4/14/2019	0.17	-4.64	26.48	0.026	0.9999	0.9999	0.9999
4/15/2019	0.32	-5.73	32.44	0.018	1.0011	1.0010	1.0011
4/16/2019	0.32	-5.04	28.54	0.029	1.0001	1.0002	1.0002
4/17/2019	0.27	-4.89	26.92	0.040	1.0000	1.0001	0.9999
4/18/2019	0.02	-3.60	20.91	0.040	1.0004	0.9999	0.9998
4/19/2019	0.49	-6.71	35.99	0.017	1.0003	1.0009	1.0008
4/21/2019	0.06	-2.85	18.03	0.046	0.9999	1.0000	1.0001
4/22/2019	0.43	-4.55	25.89	0.039	0.9999	1.0002	1.0002
4/23/2019	0.47	-4.58	28.93	0.046	1.0008	1.0006	1.0006

Appendix F – BenthoTorch Chl-*a* Data

8.6.1 Data Collection

Benthic chlorophyll-*a* (Chl-*a*) concentration was measured in both streams between August 2018 and June 2019, 12 times in Oak Creek (Figure F1a) and 13 times in South Fork Mill Creek (Figure F1b). Chl-*a* concentrations were measured using a BBE Moldaenke BenthoTorch, a handheld fluorimeter that measures chl-*a* in situ. Chl-a concentration was measured in four regions in each stream. Two regions were located in bends of the stream, while the other two were located in straight sections. The regions were chosen to have substrate grains large enough for the BenthoTorch to create a seal around the sensor when taking measurements. In Oak Creek, 15 measurements were taken in each location. In South Fork Mill Creek, 20 measurements were taken in each location and were split into two subregions. These regions were split by relative grain size – one subregion with smaller grains and one with larger grains.

Each sampling region is located between two cross sections surveyed in the stream (Table F1). The downstream-most region was named BT1, while the upstream-most region was named BT4, with BT2 and BT3 in between, in order. In South Fork Mill Creek, the regions were split into subregions (Table F2). The sampling regions were marked by flagging along the stream banks.

During each sampling event, the measurements were taken on random rocks within the region. These grains were chosen by the measurer because a) the grain was large enough that a sensor-sized region could be covered by the BenthoTorch, b) they grain did not have a cover of sediment on its surface, c) the grain was not buried beneath other grains, and d) there were no invertebrates on the grain surface. Each sampling campaign began at the downstream end of the stream reach to ensure that the benthic periphyton had not been recently disturbed. Measurement within the region also began at the downstream end for the same reason.

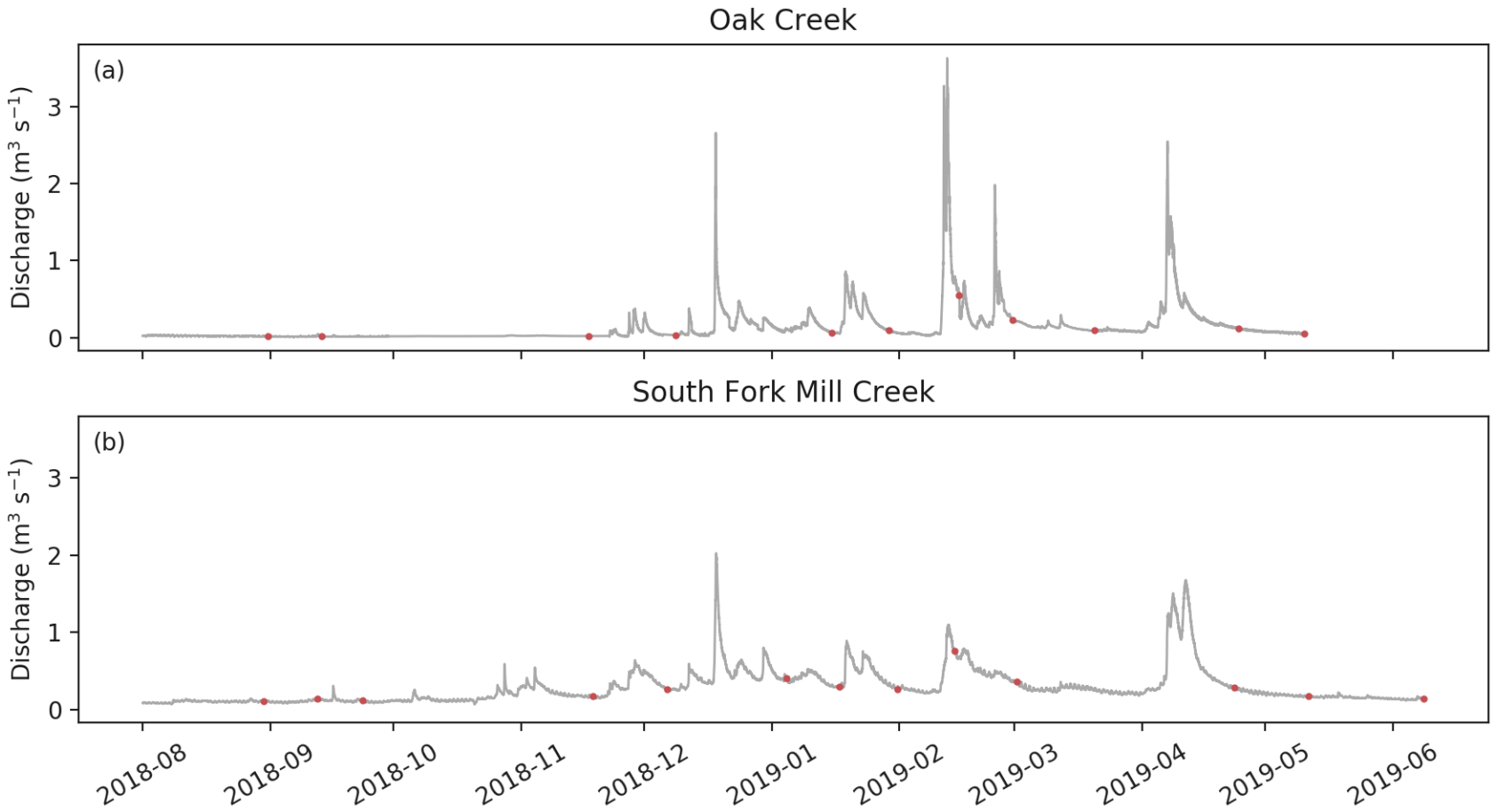

Figure F.1 BenthoTorch Chl-*a* concentration sampling events from August 2018 to May 2019 in Oak Creek (a) and South Fork Mill Creek (b). Measurements were made on 11 dates in Oak Creek, during periods with discharges between 0.02 m^3 s^{-1} and 0.55 m^3 s^{-1}. Measurements were made on 13 dates in South Fork Mill Creek, during periods with discharges between 0.11 m^3 s^{-1} and 0.76 m^3 s^{-1}.

Table F.1 Description of sampling location boundaries in Oak Creek and South Fork Mill Creek.

BenthoTorch Region	Cross Section Boundaries, Oak Creek	Cross Section Boundaries, South Fork Mill Creek
BT1	XS 11-13	XS 29-30
BT2	XS 23-25	XS 22-23
BT3	XS 38-40	XS 11-12
BT4	XS 46-48 (upstream of culvert)	XS 3-5

Table F.2 Description of relative locations of small- and large-grain sampling locations in each BenthoTorch region of South Fork Mill Creek.

BenthoTorch Region	Small Grain Sampling Location	Large Grain Sampling Location
BT1	Close to right bank	Between small grains and thalweg
BT2	Close to left bank, above drop into pool	Along right bank
BT3	Along right bank	Between thalweg and left bank
BT4	On right side above drop into pool	Along thalweg

8.6.2 Data Summary

The data collected are located in the Segura_Lab folder in the T: drive, in the location T:\Groups\Segura_Lab\2017_Sediment_Transport_Ecology\Chla\BenthoTorch_Data. The data are all collected in an Excel workbook called “All Data.xlsx” with individual sheets for each sampling event. There are also individual .csv files saved for each sampling event. This folder also includes the Python Jupyter Notebook code for plotting the data, as well as the saved .png and .pdf files from running the code.

The quartiles of the distribution of total chlorophyll-a concentration measured during the sampling date shown in a box-plot for both creeks (Figure F2, Figure F3). The mean and standard deviations of the concentration data are also shown for each creek (Figure F4, Figure F5). The two creeks are compared, with the mean and standard deviation of the two closest sampling dates plotted together (Figure F6). The data spreadsheets also contain information about relative grain size and the morphology of the stream in the sampling region for each measurement, which can be used when comparing between and within sites.

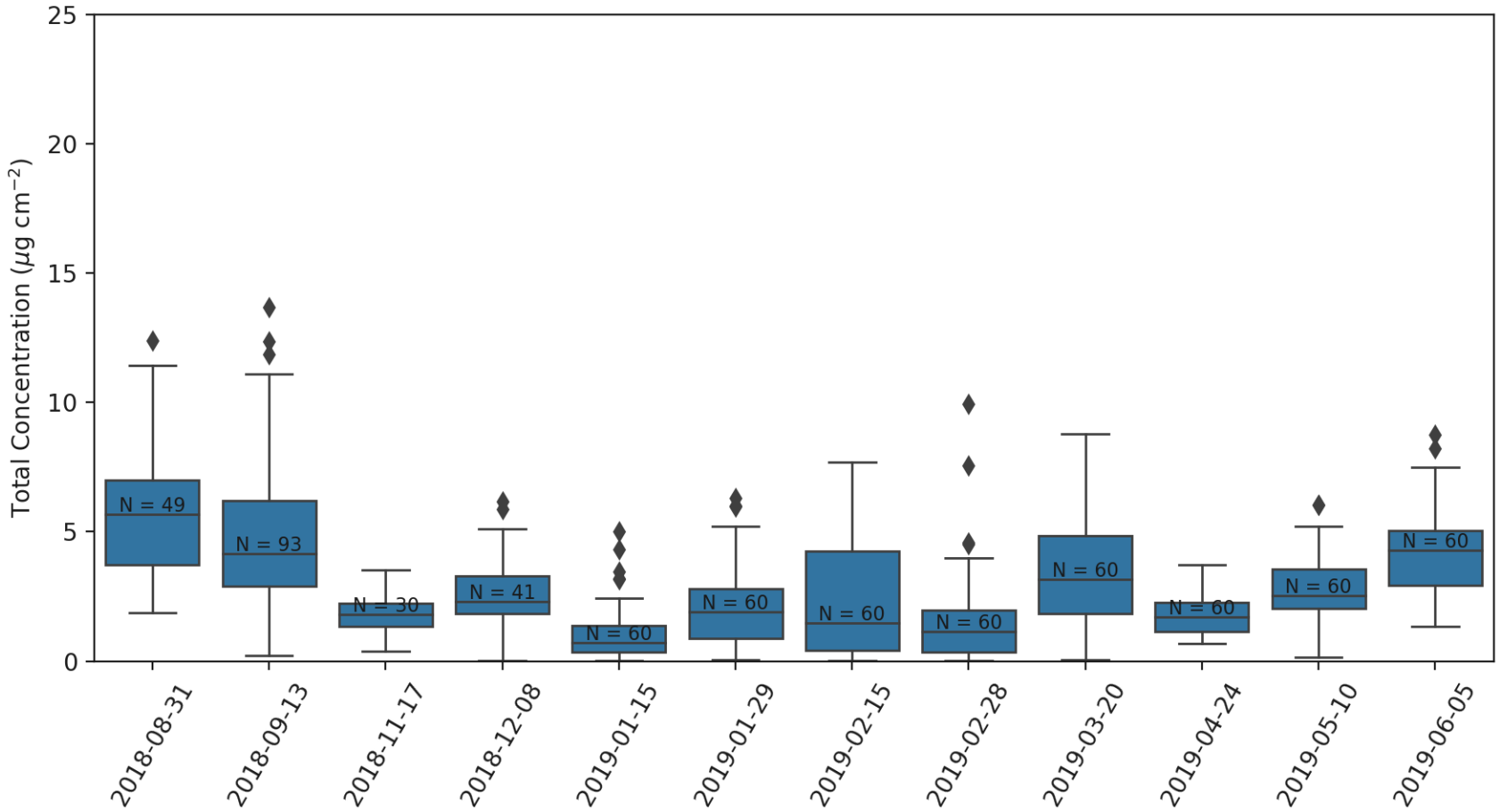

Figure F.2 Range in total concentration per measurement of collected data in Oak Creek over the period from August 2018 to June 2019. N shows the number of measurements made on that date.

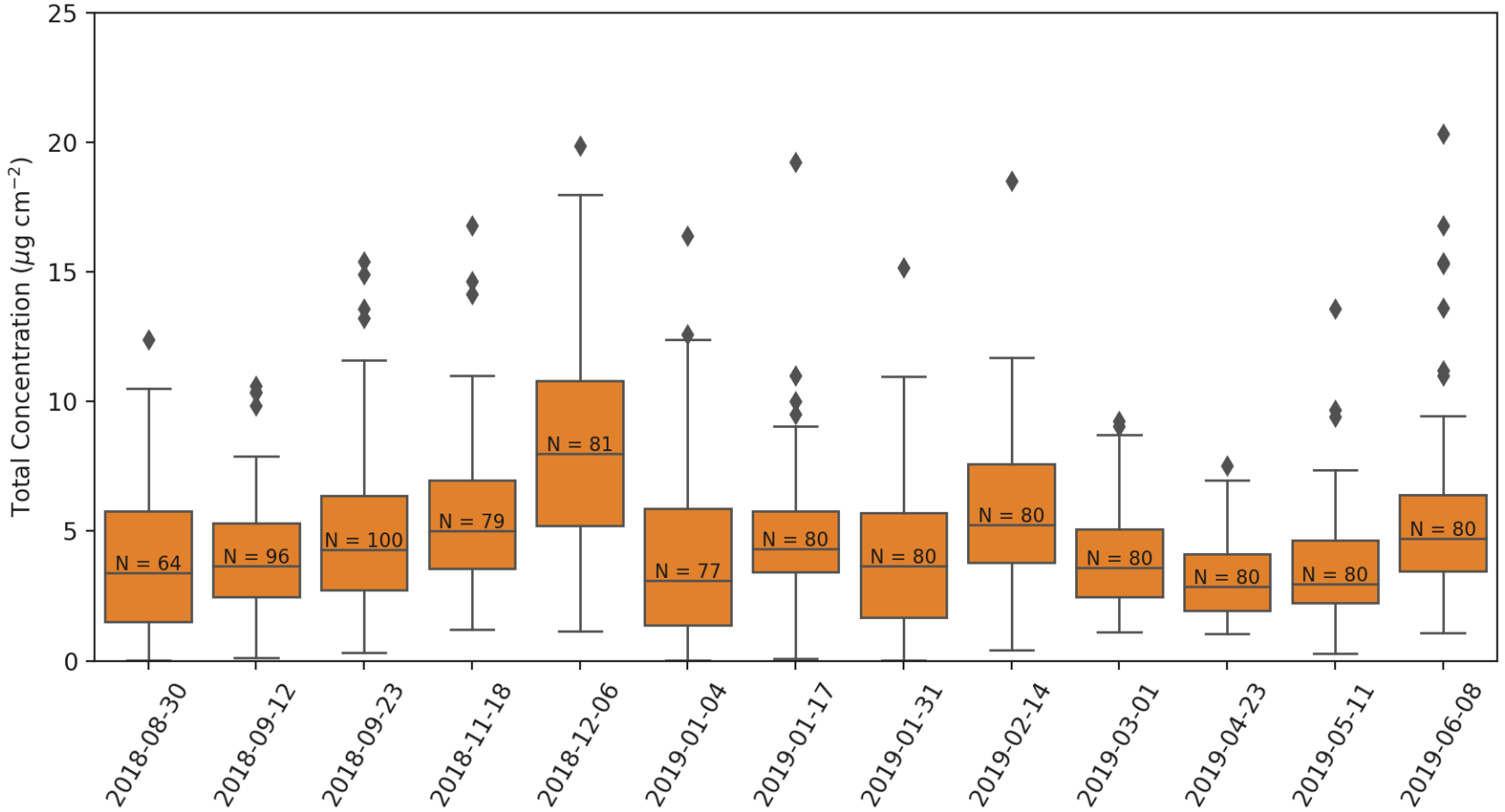

Figure F.3 Range in total concentration per measurement of collected data in South Fork Mill Creek over the period from August 2018 to June 2019. N shows the number of measurements made on that date.

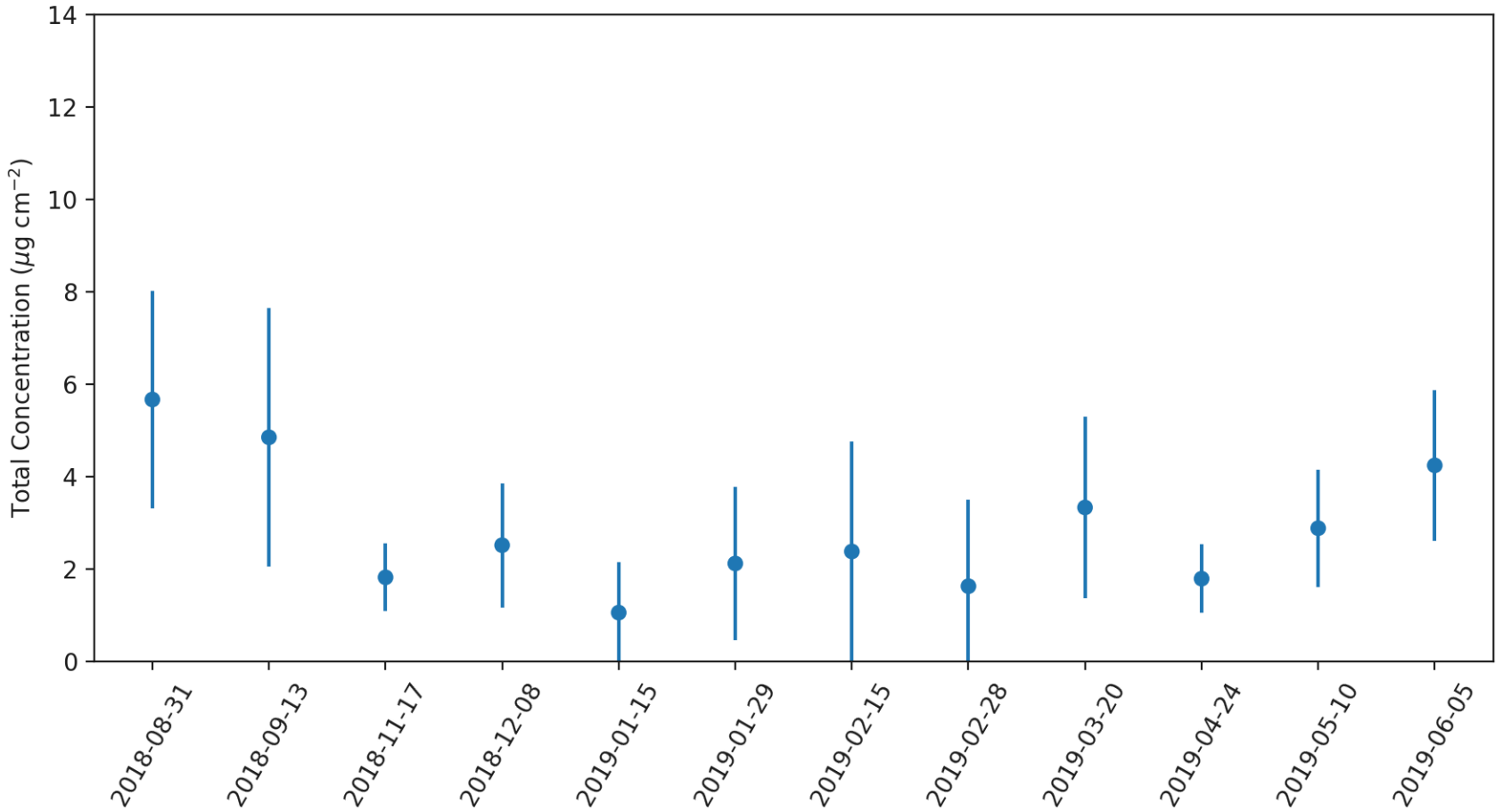

Figure F.4 Average and standard deviation of total concentration measured per event in Oak Creek over the period from August 2018 to June 2019.

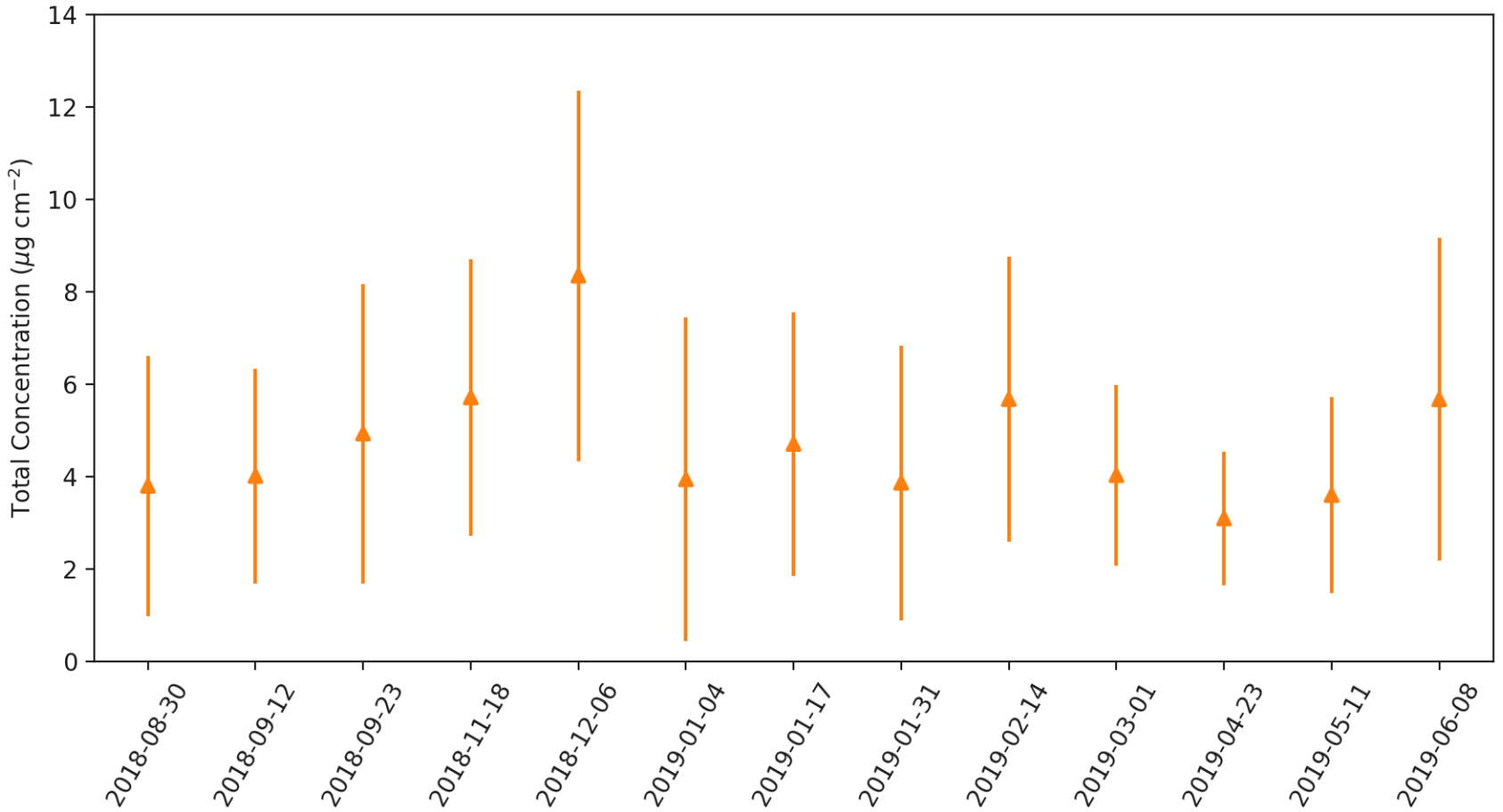

Figure F.5 Average and standard deviation of total concentration measured per event in South Fork Mill Creek over the period from August 2018 to June 2019.

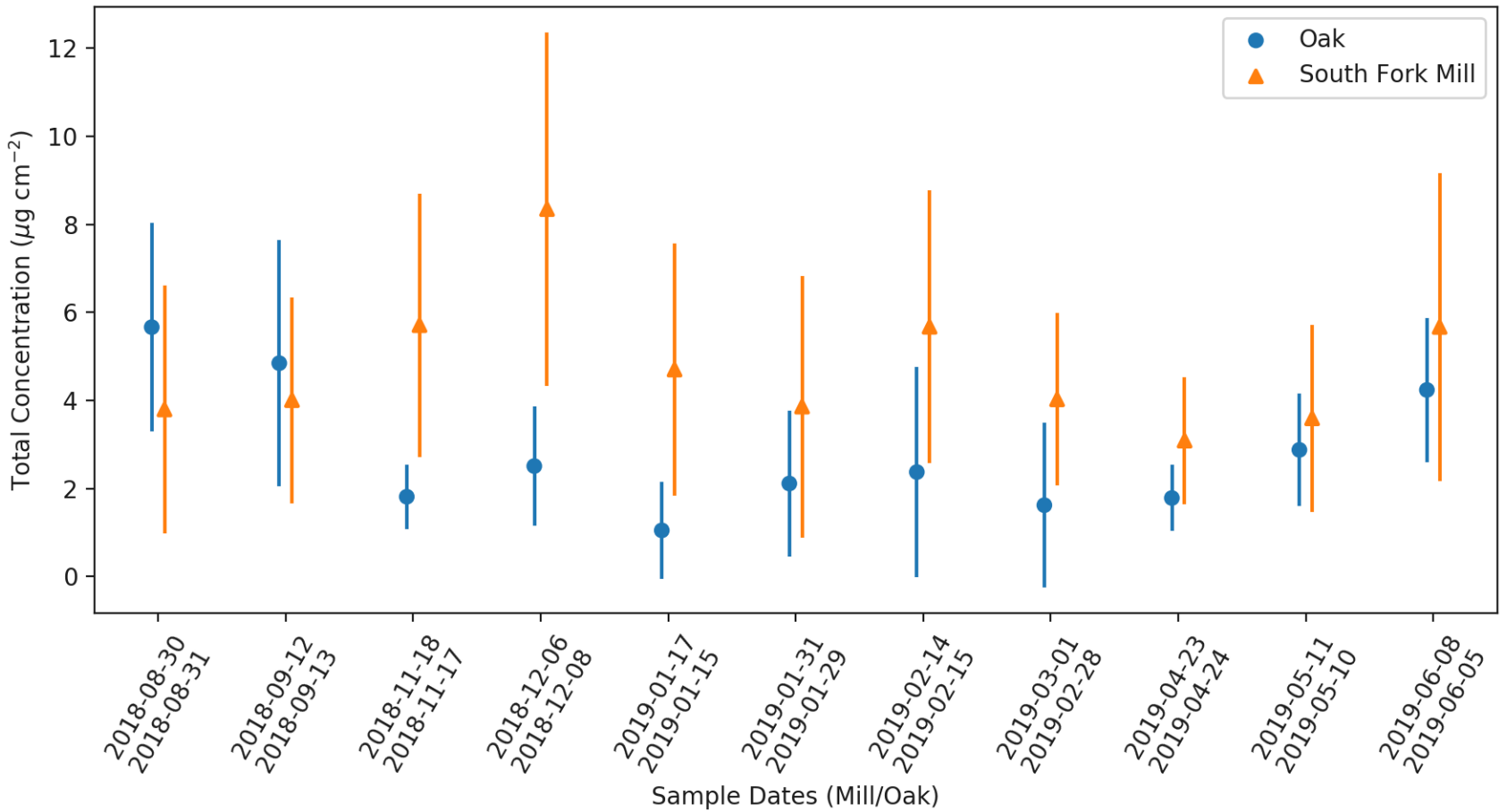

Figure F.6 Comparison between average total concentrations measured per event in Oak Creek versus South Fork Mill Creek over the period from August 2018 to June 2019.

Appendix G – Collected Topography Data

8.7.1 Data Collection

A detailed topography survey of South Fork Mill Creek was conducted using a Nikon Nivo5.C Total Station between June and August 2018. 42 cross sections were installed along the reach by pounding wooden stakes in on the banks past the bankfull elevation. Cross section stakes are labeled with pink/black striped flagging, and have attached metal labels with cross section numbers. Cross sections were installed about 1.5 bankfull widths apart. Cross section survey points were surveyed by hanging a measuring tape between the stakes, stretching across the stream. Additional survey points were added between cross sections in the active channel and on the banks in order to better characterize topography when interpolating the data to create a topographic map of the reach. Points were surveyed with a density of about 1.8 points/meter^2, and a total of 3,012 points were surveyed (Figure G1).

Topography data were also collected in Oak Creek using the same Total Station between August and September 2017. 49 of the previously installed cross sections were surveyed, with a total of 1,275 points collected (Figure G2).

8.7.2 Data Summary

Survey data are located in the Segura_Lab folder in the T: drive, in the location T:\Groups\Segura_Lab\2017_Sediment_Transport_Ecology\Surveying_Data\Mill\Mill_csv_files. All topography points are in the file "Mill_TopoPoints.csv" with subset files of "Mill_wet.csv" for points of the wetted extent, and "Mill_XS_only.csv" for points on the cross sections. Points are labeled with a description of the point type in the main topography file. The points are labeled with some combination of the codes represented in Table G1. Data for Oak Creek are in the same Surveying_Data folder in the Oak\Oak_csv_files subfolder. Files are labeled similarly, and points are labeled with the same scheme as in Table G1.

Table G.1 Topography survey point label meanings

Code	**Meaning**
xs#	Cross section
ep	Extra point
lw, rw	Left wetted extent, Right wetted extent
lb, rb	Left bank, Right bank
top	Top of survey pin
bop	Bottom of survey pin
log	Point taken on a log
eol	End of log

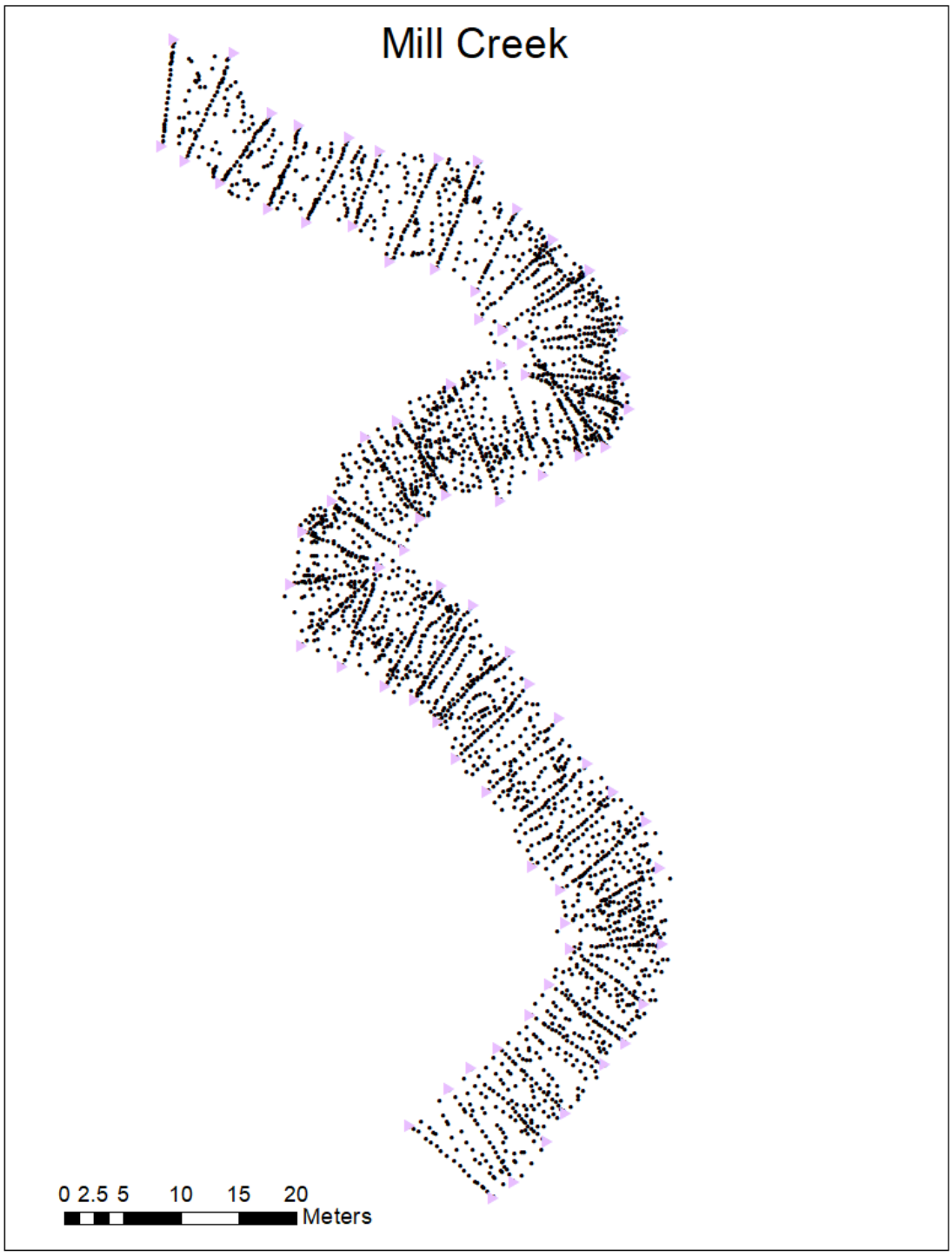

Figure G.1 Collection of all topography survey points taken at South Fork Mill Creek. Purple triangles represent cross section pins installed on the banks.

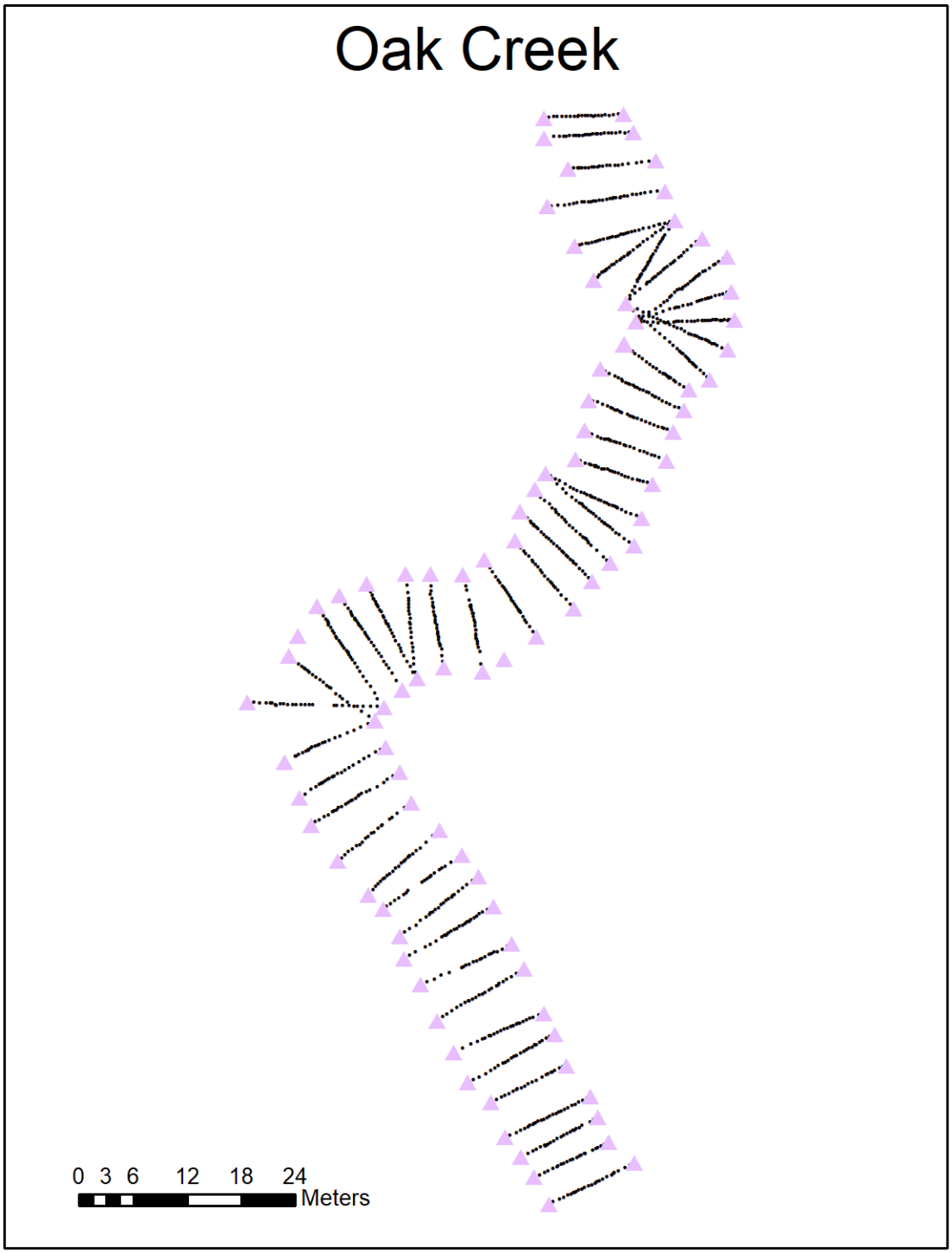

Figure G.2 Collection of all topography survey points taken at Oak Creek. Purple triangles represent cross section pins installed on the banks.

Appendix H – Bedload Sampling Data

8.8.1 Data Collection

From 2017 to 2019, several bedload samples were collected at Oak Creek. Samples were collected either in the downstream concrete weir, or from the bridge over the stream. Samples were collected with the modified Elwha sampler. From the concrete weir, one person stood in the weir holding the sampler. From the bridge, one person held the sampler on the downstream edge of the bridge using the long rod, while another held tension on a rope attached to the sampler, threading under the bridge and up on the upstream edge to keep the sampler from being pushed downstream by the force of the water. To collect samples, the sampler was moved along a cross section across the stream and held in place at each location for a given time interval. Once the full cross section was complete, the entire composite sample was poured into a mesh bag to dry out. Once dry, samples were poured into labeled Ziploc bags to await further analysis.

8.8.2 Data Summary

Table H.1 Bedload sample collection summary

Date	Time (PST)	Locations Along Cross Section	Time at Location (min)	Weir or Bridge Sample	Staff Gage (ft)
1/23/18	20:08-20:22	14	1	Weir	0.54
1/27/18	8:06-8:41	17	2	Weir	0.57
2/25/18	15:06-15:48	17	2	Weir	0.68-0.76
4/8/18	10:19-10:55	17	2	Weir	0.82
2/12/19	8:24-8:51	17	2	Weir	0.76-0.79
2/12/19	10:43-11:08	12	2	Bridge	1.0-1.05
2/12/19	16:38-17:10	12	2	Bridge	1.15

Appendix I – Nighttime Regression Method

We explored the use of a nighttime regression method to calculate gas exchange rates (K_O) from our daily O_2 data. Photosynthesis by primary producers during the day results in O_2 being out of equilibrium when the sun sets and night begins. Once photosynthetic processes stop for the day, the rate of return to equilibrium is a function of the gas exchange rate:

$$\frac{\Delta O}{\Delta t} = ER + K_O(O_{sat} - O) \quad (8.1)$$

When the rate of change in O_2 and the O_2 saturation deficit are plotted using O_2 data from the time immediately after photosynthesis stops, the slope of the resulting line is the gas exchange rate for oxygen.

We used a code to find the best-fit solution for K_{600} for every day with data, using the above equation. The code requires a dataset with times, water temperatures, dissolved oxygen concentrations, and saturated dissolved oxygen concentrations. The code regresses over a series of time windows varying around the time of sunset to find the best-fit line between rate of change of O_2 and O_2 saturation deficit. With this best-fit line, the calculated slope is converted to K_{600}, a normalized gas exchange rate. We experimented with running 1-hour and 2-hour windows, starting the regression windows at 5:00 PM and allowing the windows to cycle through 4 window options, which begin at 5:00, 6:00, 7:00, and 8:00 PM. The output from the code includes the slope, a K_{600} value, and an r^2 for the fit of the line. An r^2 value cutoff must be used to determine which K_{600} values might be reasonable. The code is not able to calculate a slope accurately if the O_2 change is too rapid or unclear.

The R code we used is located in the Segura_Lab folder in the T: drive, in the location T:\Groups\Segura_Lab\2017_Sediment_Transport_Ecology\Nighttime_Regression. The folder includes initial experiments running the code with data from Oak Creek and South Fork Mill Creek.